D 2.2

Report on heat powered cooling technology assessment

APRE

UNIVERSITÀ DEGLI STUDI FIRENZE | DIEF DIPARTIMENTO DI INGEGNERIA INDUSTRIALE

COSVIG

SDU

Geothermal UKRAINE

SINTEF

RIVACOLD MASTERING COLD

neo-eco

FORMAGGERIA TOSCANA

www.geosynproject.eu

info@geosynproject.eu

#GEOSYNPROJECT

Funded by the European Union

D 2.2	**Report on heat powered cooling technology assessment**
DELIVERABLE TYPE	Report
MONTH AND DATE OF DELIVERABLE	Month 12, 31/10/2025
WORK PACKAGE	WP2 Thermal Design for Optimal Energy Cascade Utilisation
LEADER	UNIFI
DISSEMINATION LEVEL	PU - Public
PROGRAMME	HORIZON EUROPE
GRANT AGREEMENT	101172812
START	1 November 2024
DURATION	36 Months

GEOSYN has received funding from the EU's Horizon Europe research and innovation programme under Grant Agreement no. 101172812.

Contributors

NAME	ORGANISATION
Adriano Milazzo	**UNIFI**

Peer Reviews

NAME	ORGANISATION
Lorenzo Talluri	**UNIFI**
Sigurd Sannan	**SINTEF ER**

Document Log

VERSION	ORGANISATION	REVIEWER	MODIFICATIONS
V 1.0	15/10/2025	Adriano Milazzo	Created the initial draft and defined the overall document structure

Funded by the European Union. Views and opinions expressed are however those of the author(s) only and do not necessarily reflect those of the European Union or the European Climate, Infrastructure and Environment Executive Agency (CINEA). Neither the European Union nor the granting authority can be held responsible for them.

Index of Contents

1 Introduction 7
1.1 Purpose and Objectives 7
2 System definition 9
2.1 Analysis of working conditions 9
2.2 Ejector cooling system 10
2.3 Design of the steam ejector 11
2.4 CRMC design 19
2.5 Design of the motive nozzle 26
2.6 Design of mixing chamber 28
2.7 Design of the end section 30
2.8 Assembly of the complete ejector 31
2.9 Expected performance of the cooling cycle 31
2.10 Role of wall roughness and heat exchange 33
3 Design of the flash evaporator 36
3.1 Motivations for a flash evaporator 36
3.2 Design constraints 37
3.3 Design results 37
4 Design of the condenser 39
4.1 Design constraints 39
5 Design of the system layout 40
6 Conclusions 41
7 References 41

Partners short names

APRE	AGENZIA PER LA PROMOZIONE DELLA RICERCA EUROPEA
UNIFI	UNIVERSITA DEGLI STUDI DI FIRENZE
COSVIG	CONSORZIO PER LO SVILUPPO DELLE AREE GEOTERMICHE
SDU	SYDDANSK UNIVERSITET
GU	NGO GEOTHERMAL UKRAINE
SINTEF	SINTEF AS
SINTEF ER	SINTEF ENERGI AS
RIVACOLD	RIVACOLD SRL
NEO ECO	NEOECO DEVELOPPEMENT
S.M.F.	FORMAGGERIA TOSCANA S.R.L.

Executive Summary

The GEOSYN project aims to accelerate the integration of geothermal heating and cooling (H&C) technologies into European industrial processes, supporting the EU's decarbonization agenda and improving energy efficiency across multiple sectors. This Deliverable D2.2 presents the preliminary design of the cooling system, with special emphasis on its fundamental component, namely the steam ejector.

The choice of steam as a working fluid is of paramount importance in the framework of the GEOSYN project, as it combines zero environmental impact with absolute safety and ubiquitous availability at virtually no cost. Moreover, ejectors are robust and have no moving parts. In principle, geothermal steam can be used directly as the motive fluid in the ejector, avoiding an intermediate heat exchanger that would add cost, complexity, and thermodynamic losses.

An innovative design procedure has been applied to the ejector. The core concept is the CRMC (Constant Rate of Momentum Change) criterion for ejector design, which was originally formulated in 2002 but has been improved and tested at UNIFI over many years. Originally conceived for ideal gas behavior and frictionless flow, the method has evolved to include real gas behavior (including condensation) and viscous losses. The first improvement is especially relevant in this project because steam condenses in the motive nozzle and evaporates again during the mixing between the motive and entrained flows. This radically changes the thermodynamic conditions along the ejector; neglecting these changes would result in physically unrealistic conditions.

According to experimental results gathered at UNIFI and confirmed by other international researchers, this method improves ejector performance by as much as 20% over conventional designs. Therefore, its adoption should reduce steam consumption and/or increase the useful cooling effect of the system.

Two Bezier curves have been added at the inlet and outlet of the ejector to guarantee a smooth transition between the CRMC profile and the pipes connecting the ejector to the other components. Furthermore, two Bezier curves have also been used for the motive nozzle to generate a profile with smoothly varying slopes. The ejector geometry assembled in this way is currently being tested and optimized through CFD simulations prior to experimental testing.

Another fundamental component of the heat-powered cooling system is the flash evaporator. This device eliminates the thermal resistance between the cooling cycle and the user. The water that cools down by evaporation is sent directly to the user without any intermediate fluid. This is feasible only if the cooling requirements are limited to above-zero temperatures, as in the case of the GEOSYN project or any other positive-temperature refrigeration application (fresh food, air conditioning, etc.).

Alternatively, the addition of a separate circuit carrying a different fluid within the flash evaporator is another possibility that does not compromise the project's validity.

The flash evaporator is directly connected to the ejector inlet, avoiding any bends or changes in diameter. In this way, the pressure loss between the evaporator and the entrance of the entrained flow is negligible. This has been achieved by introducing the motive fluid from the side. However,

the 90° angle will not cause significant pressure losses for the motive fluid, given its lower specific volume.

Finally, the condenser has been selected from commercially available units. The chosen device features a large-diameter intake port, which allows a direct connection to the ejector discharge. Again, this helps to reduce pressure losses and increases the capability of the ejector to overcome high discharge pressures (i.e., high condensation temperatures).

1 Introduction

The GEOSYN project aims to foster the integration of innovative geothermal technologies into European industrial processes, facilitating a sustainable energy transition while enhancing energy efficiency and reducing greenhouse gas (GHG) emissions. The project focuses on the synergistic integration of geothermal H&C systems within a broad range of industrial sectors, capitalizing on Europe's diverse geothermal potential. By targeting industrial processes with substantial H&C demands, GEOSYN aspires to optimize energy use, support decarbonization strategies, and contribute to EU climate targets.

This deliverable D2.2 focuses on the Heat Powered Cooling System (HPCS), which is first analyzed as a stand-alone system in order to optimize it. Once optimized and tested, the cooling system will be integrated with the High-Temperature Heat Pump (HTHP) and the synergy between the two functions, heating and cooling, will be fully exploited.

The activities presented in D2.2 are part of Task 2.2 (M1–M12), led by UNIFI with the active participation of RIVACOLD. The task focuses on the heat-powered cooling system, designed to harness the cascading benefits of geothermal energy and the subcooling of the HTHP.

1.1 Purpose and Objectives

The main purpose of Deliverable D2.2 is to present a detailed thermodynamic modelling of the heat-powered cooling system, which eventually leads to a design of its fundamental components and an evaluation of its performance.

The specific objectives of D2.2 are:

- Analysis and discussion of the working conditions for the heat powered cooling system. These working conditions are being continuously measured at S.M.F in order to gather average as well as extreme values that will be encountered during the on-site experimental phase. A representative set of working conditions will be also reproduced by RIVACOLD in their premises for the laboratory test phase.
- Design of the steam ejector which is the most relevant component of the cooling system and ultimately determines its global performance.
- Design of the flash evaporator, which acts also as liquid receiver, i.e., fluid reservoir that guarantees a smooth operation during transients.

- Design of the condenser, which should present the lowest possible thermal resistance between the condensing steam and the heat sink, to avoid limitations for the ejector functionality.
- Selection of other components, i.e., valves, piping, etc.
- Design of the system layout for the laboratory test phase. This layout will be reproduced on S.M.F premises with necessary modifications to adapt the system to the specific needs of the on-site operation.

By fulfilling these objectives, D2.2 represents a fundamental step towards the practical demonstration of the GEOSYN concept potential.

2 System definition

This chapter outlines structure of the cooling system, its specification and the design of the most relevant component, i.e., the ejector.

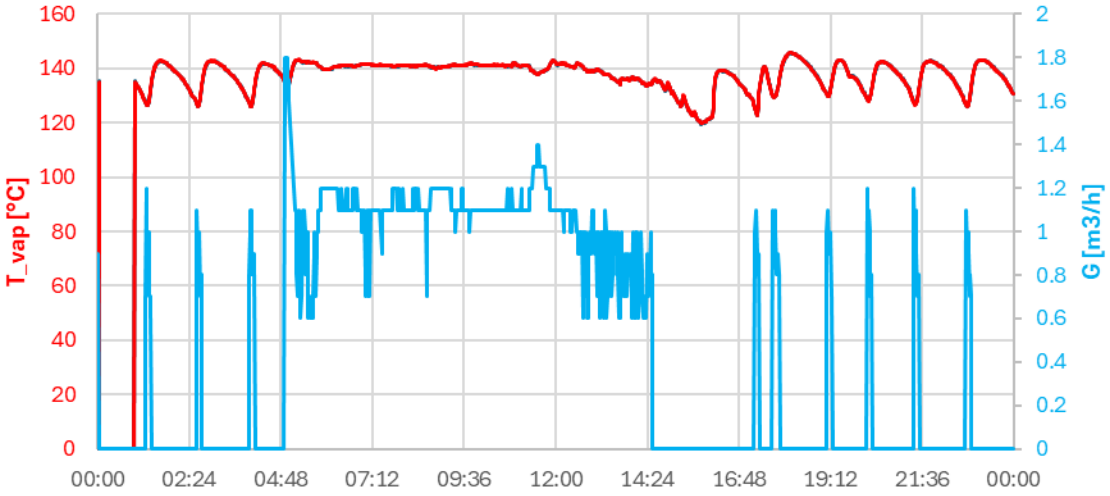

Figure 1 Data collection at S.M.F.

2.1 Analysis of working conditions

A set of instruments has been installed at S.M.F in order to collect the fundamental data along a significant period of operation (Figure 1). A typical result is shown in the same figure.

The steam flow comes from a geothermal power plant through a pipe approximately 500 m long. As can be seen, the steam temperature is typically between 120°C and 140°C. In full operation, the steam flow rate is between 1.0 m^3/h and 1.2 m^3/h, and has a temperature of 140 °C. Given that the pipe is relatively long and the insulation is not perfect, it may be assumed that the steam arrives at the S.M.F premises in saturated conditions.

The S.M.F factory returns the condensate from all its production processes to the geothermal power plant at temperatures between 15°C and 20°C.

The system will be designed to deliver a cooling power of 20 kW.

2.2 Ejector cooling system

The proposed cooling system is based on a supersonic steam ejector and a flash evaporator that directly produces the chilled water for the user. A simple scheme is shown in Figure 2.

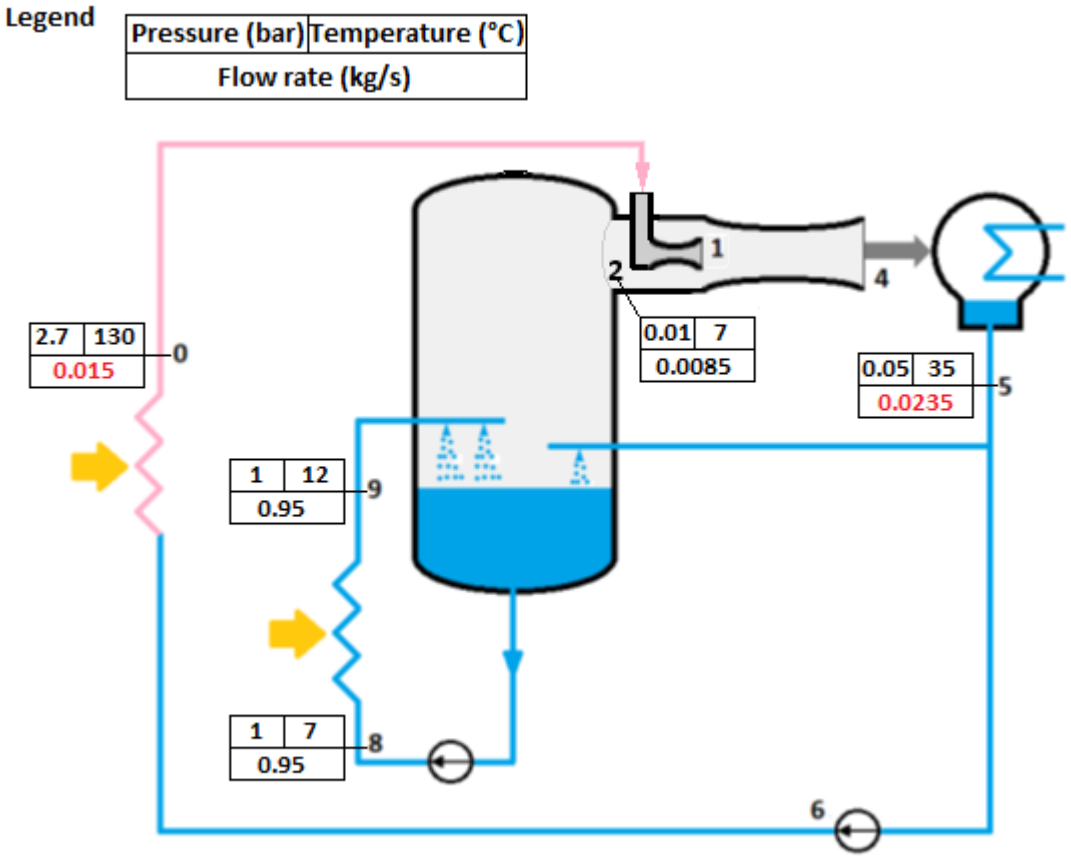

Figure 2 Scheme of the cooling system

The ejector receives hot steam from the geothermal source and expands it in a supersonic nozzle down to a low pressure and temperature (state 1). Exiting from the nozzle, this motive steam entrains the low-temperature steam from the flash evaporator in section 2. The two flows mix and recover pressure from their kinetic energy, hence reaching the condenser pressure in the exit section 4. The liquid collected in the condenser (state 5) is then divided into two flows: one equal to the entrained flow (section 2), which is sprayed within the flash evaporator, and the other forming the motive stream. This latter is pumped to the hot heat exchanger at the geothermal source.

The cooling load is served via another pump that brings the water from the flash evaporator to atmospheric pressure (state 8). This prevents air infiltration and compensates for head losses along the circuit. The resulting pressure in 9 is used to spray the water inside the flash evaporator.

2.3 Design of the steam ejector

The design of steam ejectors is a well-established process and reflects the long experience accumulated on the manufacturing of these devices. The development of ejectors can be traced back to around 1850, when the French inventor Henri Giffard formulated the basic principle of the steam injector, deriving a momentum equation that remains fundamentally valid today. The injector became a fundamental component in steam locomotives (Figure 3). This apparatus drew considerable attention at the time, as it was able to pump water into the boiler pressure using steam at the same pressure of the boiler. Notably, the spindle could be manually operated to adjust the area of the motive nozzle D. This concept has recently been "rediscovered" and may also be useful in our case.

The operating principle was easily transferred to steam ejectors, which were extensively used from the early 20th century to produce the vacuum required for the brake system on trains.

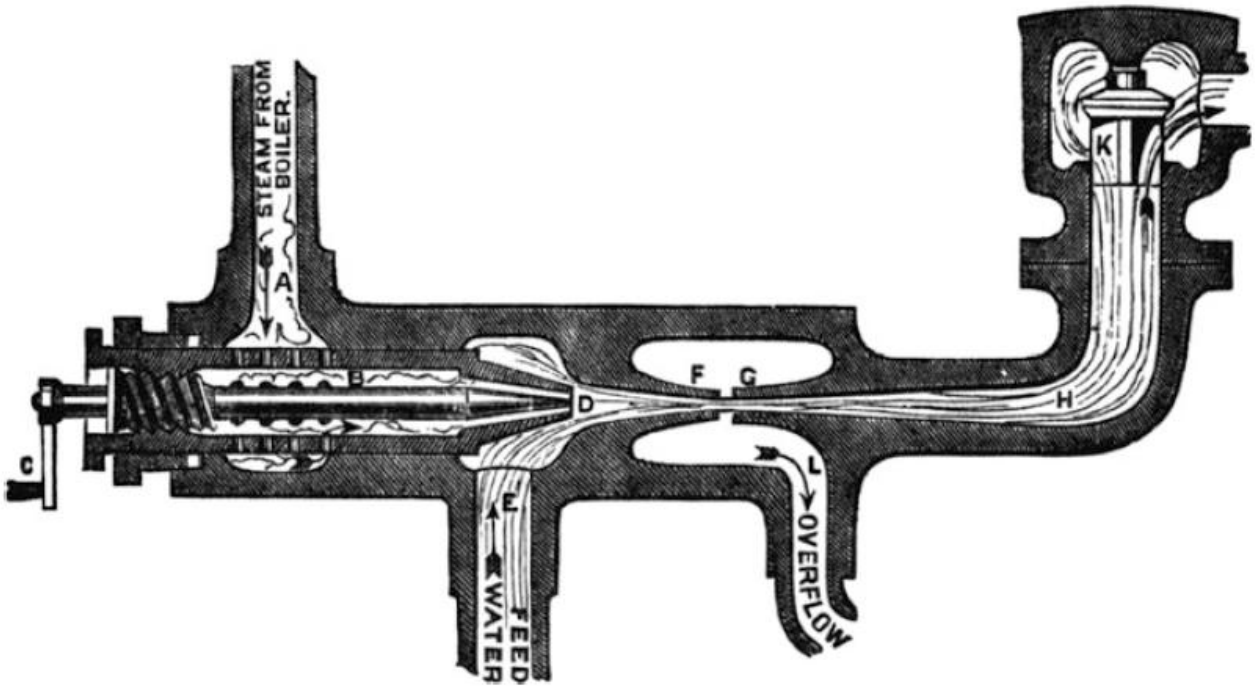

Figure 3 Giffard's injector (from Routledge, 1876)

When mechanical compressors were costly and often unreliable, refrigerants were toxic and steam was more widespread than electricity, ejectors played a significant role in the refrigeration industry. However, once these limitations were overcome — compressors evolved, Freons provided safe and efficient refrigerants, and electricity reached the majority of users — the electric refrigerator became the dominant cooling technology for all applications.

Ejectors were thereafter relegated to niche applications, such as extraction of non-condensable gases from condensers in steam power plants. Even so, several fundamental studies on the

operating principles of the supersonic ejector were published. Just to cite one, the work of Keenan (1950) has been a reference for many subsequent studies and continues to be cited today. The fundamental hypothesis of this approach — later confirmed by experiments — is a constant-pressure mixing of the motive and entrained flows. This mixing produces a supersonic flow that undergoes a normal shock in the throat (Figure 4), recovering pressure and resulting in a subsonic flow. The latter then slows down and recovers additional pressure in the diverging discharge section of the ejector.

From this and subsequent models, no direct indication is provided regarding the optimal length of the various parts of the ejector, which are instead determined empirically. This simplified modelling approach likely reflects the relatively ease of designing and constructing ejectors with satisfactory performance. Many applications are not particularly demanding in terms of ejector performance, while misconceptions persist, such as the frequent confusion between ejectors and simple Venturi convergent-divergent devices.

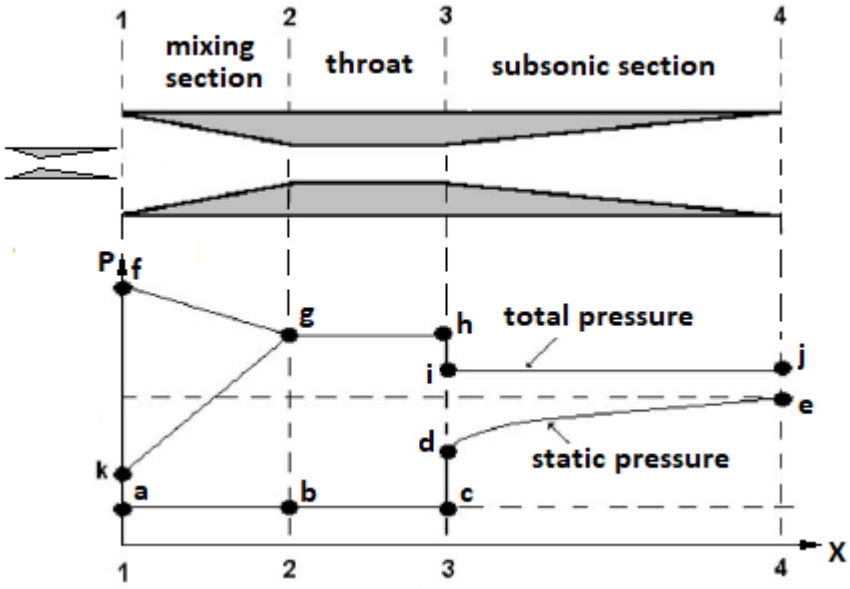

Figure 4 Constant pressure mixing model

When it comes to heat-powered refrigeration, however, efficient ejector operation becomes crucial. The availability of highly efficient absorption chillers poses a benchmark that is very difficult to surpass. Meanwhile, advanced analysis tools such as computational fluid dynamics (CFD) have become widely accessible, leading to a deeper understanding of the ejector behaviour.

This has stimulated significant scientific activity on ejectors, although the transfer of knowledge from theoretical studies or lab-scale experiments to industrial manufacturers of ejectors has remained somewhat limited. For a comprehensive review of the literature on ejectors, see, for example, Besagni (2016).

Since the early 2000s, a research group led by Professor Giuseppe Grazzini at the University of Florence has designed and built an advanced steam ejector prototype featuring several noteworthy characteristics, including a flash evaporator and a double stage configuration (Grazzini, Rocchetti, 2002). In the same year, Professor Ian W. Eames at University of Nottingham proposed a thermodynamic criterion for ejector design known as CRMC (Constant Rate Momentum Change) (Eames, 2002). Among the research groups that identified promising potential in the approach of Eames were those of Volodymyr Petrenko at Odessa State Academy of Refrigeration in Ukraine, Satha Aphornratana at the Sirindhorn International Institute of Technology in Thailand, and Giuseppe Grazzini in Florence.

Research on CRMC ejectors in Florence gained momentum in 2010, when the industrial partner Frigel S.p.A. became involved and a full-scale prototype ejector chiller was constructed (Figure 5). Professor Eames directly contributed to the design of the prototype. The ejector underwent several subsequent improvements (last version shown in Figure 6), and finally, in 2015, convincing experimental performance was achieved, supported by detailed CFD analyses that revealed new insights into ejector operation (Mazzelli, Milazzo, 2015).

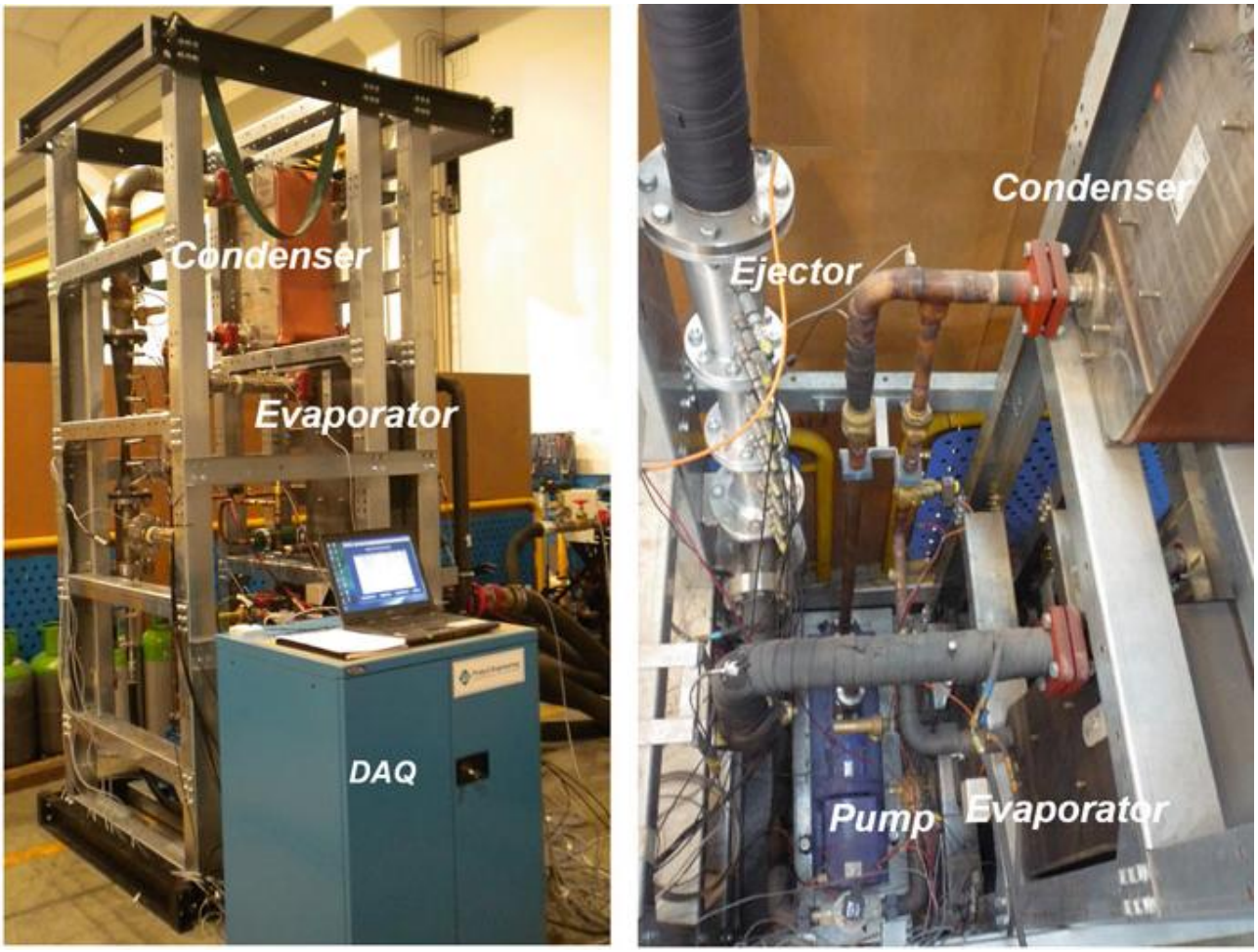

Figure 5 Ejector chiller prototype designed at UNIFI

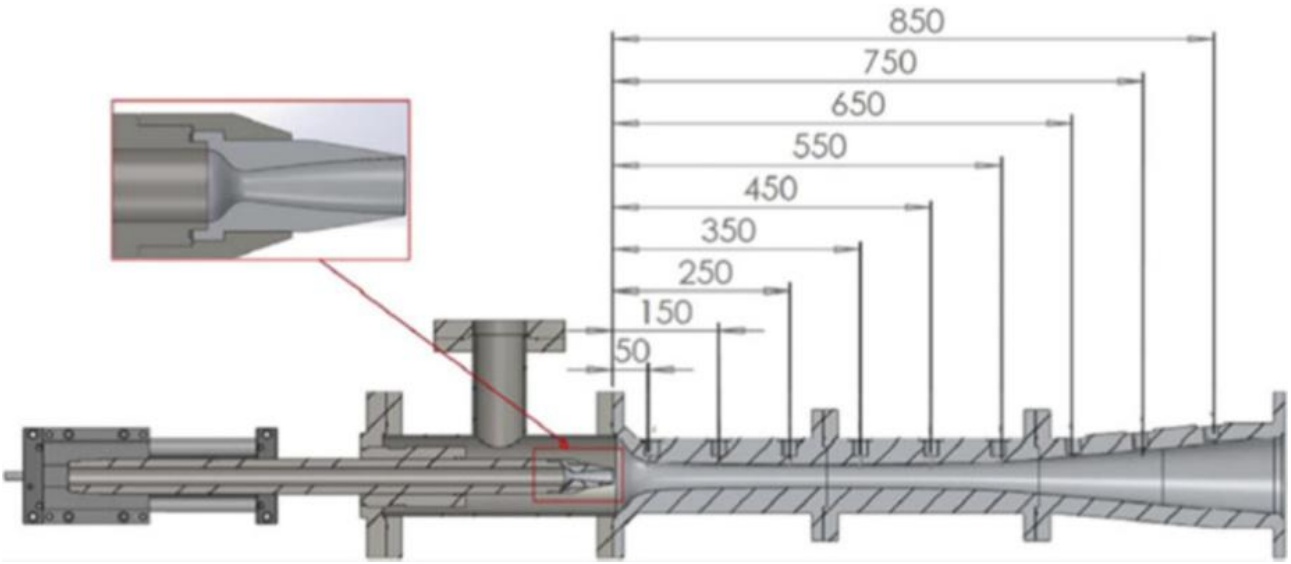

Figure 6 Last version of the UNIFI ejector

The research activity on the prototype continued until 2021. In the initial phase, R24fa was selected as the working fluid due to its favourable thermodynamic characteristics. Later, new results were obtained using a low-GWP refrigerant (R1233zd). An example of these results is shown in Figure 7 (Mahmoudian, Mazzelli, Rocchetti, Milazzo, 2021).

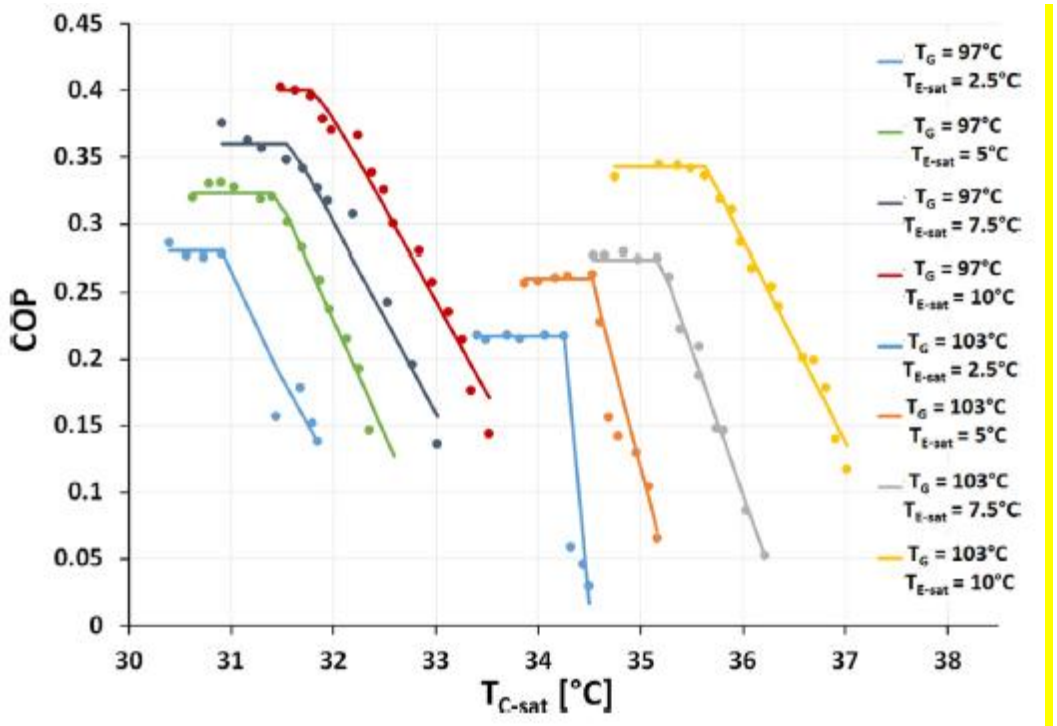

Figure 7 Performance of the UNIFI ejector chiller (Mahmoudian et al., 2021)

Figure 7 illustrates the typical behaviour of an ejector chiller. Taking, for example, the yellow curve at the right side of the figure, the COP remains fairly constant up to a certain value of the saturation temperature at the condenser (around 35.5°C in this case). When this critical temperature is exceeded, the performance decreases sharply. This behaviour confirms the existence of a chocked condition inside the ejector, which makes it insensitive to the outlet conditions up to a certain critical discharge pressure. The critical pressure (or, equivalently, the saturation temperature) therefore represents the second fundamental performance parameter of the ejector chiller, as it limits its operation in warm climates. The situation worsens as the saturation temperature at the evaporator is reduced: the four curves on the right show the COP for $T_{E\text{-}sat}$ decreasing from 10°C (yellow curve) to 2.5°C (light blue curve).

For a given ejector, the performance can be modified by changing the pressure of the motive flow. Here, for example, the four curves on the left show how the ejector behaves when the saturation temperature of the motive fluid is decreased from 103 °C to 97 °C. The COP values in the horizontal portion of the curves increase, but the critical condensation temperature decreases. For example, the uppermost red curve reaches a COP of 0.4, but the corresponding critical condensation temperature is below 32 °C. Again, the performance decreases as the evaporation temperature is reduced.

It is important to understand that this behaviour corresponds to a fixed ejector design. To take advantage of an increased temperature of the heat source, the ejector geometry must be modified. More specifically, the ratio between the nozzle throat area and the diffuser throat area should be reduced as the motive fluid inlet temperature is increased.

The chiller COP is directly related to the ejector **entrainment ratio,** $\omega = \frac{\dot{m}_s}{\dot{m}_m}$. As shown in Fig. 8, the cooling effect is given by the enthalpy difference $h_E - h_A$ available at the evaporator. The energy input, on the other hand, corresponds to the enthalpy difference $h_G - h_A$. This includes both the pump work (barely visible in the diagram) necessary to raise the pressure from the condenser outlet (point A) to the hot heat exchanger, plus the heat absorbed there to reach the final condition (point G). Therefore, $\dot{m}_m$ denoting the motive flow (point G) and $\dot{m}_s$, the cooling flow passing through the evaporator, the COP is:

$$COP = \frac{\dot{Q}_f}{\dot{Q}_{in} + \dot{W}_{pump}} = \frac{\dot{m}_s(h_E - h_A)}{\dot{m}_m(h_G - h_A)} \propto \omega$$

Funded by the European Union

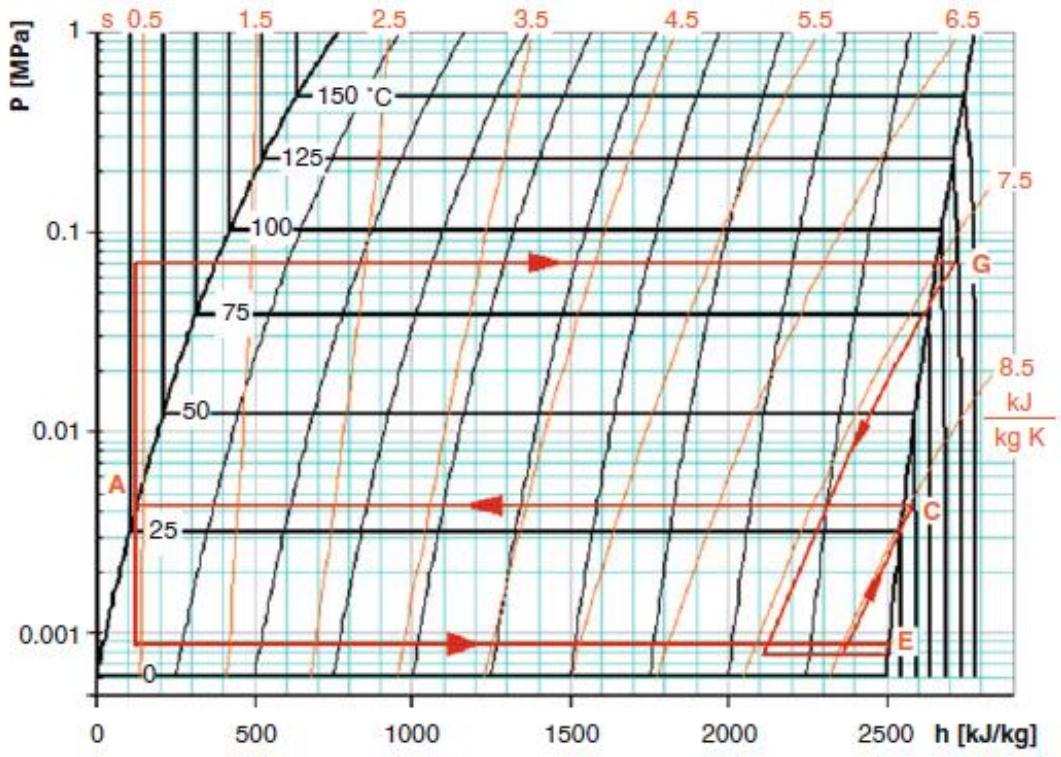

Figure 8 Pressure/enthalpy diagram of the thermodynamic cycle for a steam ejector chiller

Therefore, building an efficient ejector chiller essentially requires an ejector with a high entrainment ratio. The research group in Thailand performed numerous experiments on their small-scale CRMC steam ejector. The key contribution from this research is the direct comparison between the CRMC and the traditional design. A recent study (Kitrattana, Aphornratana, Thongtip, 2023) demonstrated that the CRMC ejector provides an average performance improvement of about 20% compared to an equivalent ejector based on conventional design criteria (Figure 9).

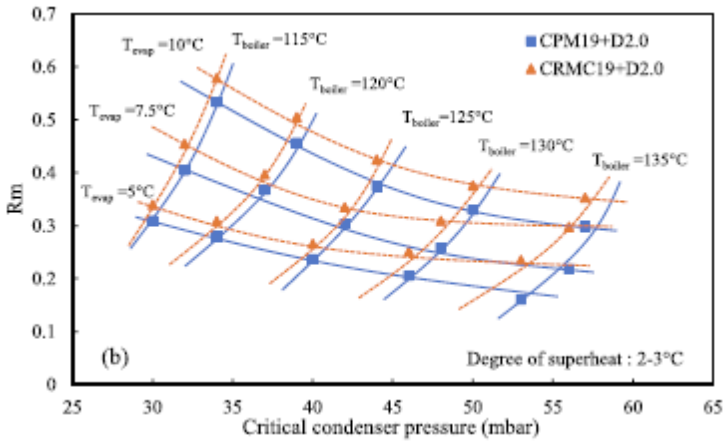

Figure 9 Performance map comparison from Kitrattana, Aphornratana, Thongtip (2023)

Therefore, when the present project was initiated, the previous work on the CRMC thermodynamic design procedure for the supersonic steam ejector was used as a starting point. To establish a benchmark, several ejector manufacturers were contacted and asked to provide quotations for an ejector meeting the required specifications (Table 1). Note that these same specifications are also assumed as the operating conditions in Figure 2.

Table 1 Ejector specifications

Cooling power	20 kW
Entrained mass flow	0.00845 kg/s (30.4 kg/h)
Entrained flow temperature	7°C
Entrained pressure (saturation)	1 kPa
Condensation temperature	35°C
Discharge pressure (saturation)	5.63 kPa
Motive steam temperature	130°C
Motive steam pressure (saturation)	2.7 bar.

Among the responses received, the most convincing offer came from Körting Hannover GmbH, that proposed a stainless-steel ejector featuring a body with DN150 suction and discharge ports. The motive steam flow rate is **70 kg/h**, and the quoted price is approximately € 15,000. As far as can be determined, the design of the ejector follows a fully traditional concept, based on the long-standing experience accumulated by this company.

Meanwhile, RIVACOLD has proposed procuring a custom-designed ejector from a manufacturer that routinely produces mechanical components for its systems. This approach will increase the innovation potential of the GEOSYN project, allowing a closer scrutiny of the ejector operation and performance.

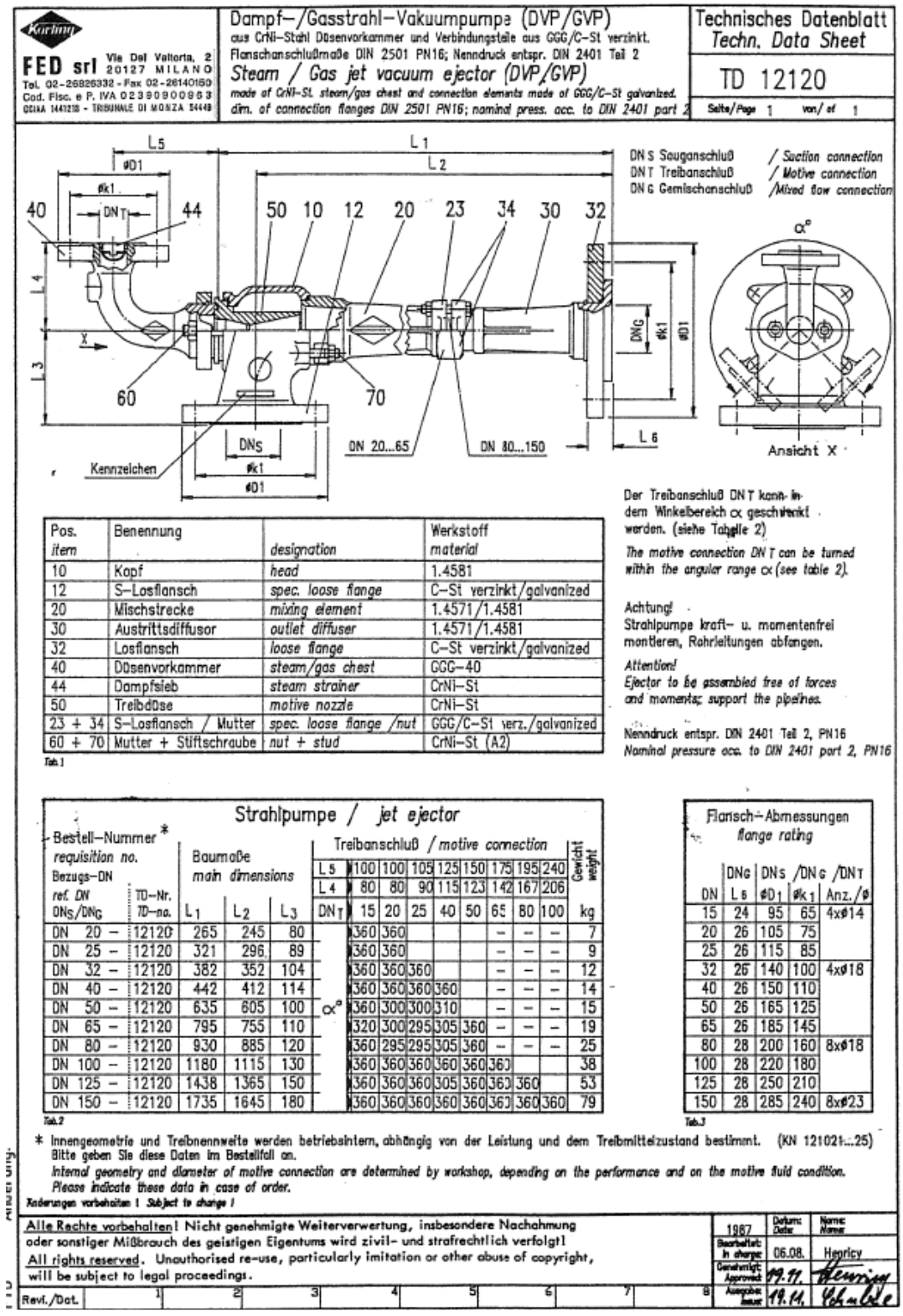

FED srl Via Del Vallorto, 2 20127 MILANO
Tel. 02-26826332 - Fax 02-26140150
Cod. Fisc. e P. IVA 02390900963
CCIAA 1441218 - TRIBUNALE DI MONZA 54448

Dampf–/Gasstrahl–Vakuumpumpe (DVP/GVP)
aus CrNi–Stahl Düsenvorkammer und Verbindungsteile aus GGG/C–St verzinkt.
Flanschanschlußmaße DIN 2501 PN16; Nenndruck entspr. DIN 2401 Teil 2
Steam / Gas jet vacuum ejector (DVP/GVP)
made of CrNi–St. steam/gas chest and connection elements made of GGG/C–St galvanized.
dim. of connection flanges DIN 2501 PN16; nominal press. acc. to DIN 2401 part 2

Technisches Datenblatt
Techn. Data Sheet
TD 12120
Seite/Page 1 von/of 1

DN S Sauganschluß / *Suction connection*
DN T Treibanschluß / *Motive connection*
DN G Gemischanschluß / *Mixed flow connection*

Ansicht X

Pos. *item*	Benennung	*designation*	Werkstoff *material*
10	Kopf	*head*	1.4581
12	S–Losflansch	*spec. loose flange*	C–St verzinkt/galvanized
20	Mischstrecke	*mixing element*	1.4571/1.4581
30	Austrittsdiffusor	*outlet diffuser*	1.4571/1.4581
32	Losflansch	*loose flange*	C–St verzinkt/galvanized
40	Düsenvorkammer	*steam/gas chest*	GGG–40
44	Dampfsieb	*steam strainer*	CrNi–St
50	Treibdüse	*motive nozzle*	CrNi–St
23 + 34	S–Losflansch / Mutter	*spec. loose flange /nut*	GGG/C–St verz./galvanized
60 + 70	Mutter + Stiftschraube	*nut + stud*	CrNi–St (A2)

Tab.1

Der Treibanschluß DN T kann in dem Winkelbereich α geschwenkt werden. (siehe Tabelle 2)
The motive connection DN T can be turned within the angular range α (see table 2).

Achtung!
Strahlpumpe kraft– u. momentenfrei montieren, Rohrleitungen abfangen.
Attention!
Ejector to be assembled free of forces and moments; support the pipelines.

Nenndruck entspr. DIN 2401 Teil 2, PN16
Nominal pressure acc. to DIN 2401 part 2, PN16

Strahlpumpe / *jet ejector*

Bestell–Nummer * *requisition no.* Bezugs–DN *ref. DN* DNS/DNG	TD–Nr. *TD–no.*	Baumaße *main dimensions* L1	L2	L3	Treibanschluß / *motive connection* L5	100	100	105	125	150	175	195	240	Gewicht *weight*
					L4	80	80	90	115	123	142	167	206	
					DNT	15	20	25	40	50	65	80	100	kg
DN 20 –	12120	265	245	80	α°	360	360				–	–	–	7
DN 25 –	12120	321	296	89		360	360				–	–	–	9
DN 32 –	12120	382	352	104		360	360	360			–	–	–	12
DN 40 –	12120	442	412	114		360	360	360	360		–	–	–	14
DN 50 –	12120	635	605	100		360	300	300	310		–	–	–	15
DN 65 –	12120	795	755	110		320	300	295	305	360	–	–	–	19
DN 80 –	12120	930	885	120		360	295	295	305	360	–	–	–	25
DN 100 –	12120	1180	1115	130		360	360	360	360	360	360			38
DN 125 –	12120	1438	1365	150		360	360	360	305	360	360	360		53
DN 150 –	12120	1735	1645	180		360	360	360	360	360	360	360	360	79

Tab.2

Flansch–Abmessungen
flange rating

DN	DNG L6	DNS ⌀D1	/DNG ⌀k1	/DNT Anz./⌀
15	24	95	65	4x⌀14
20	26	105	75	
25	26	115	85	
32	26	140	100	4x⌀18
40	26	150	110	
50	26	165	125	
65	26	185	145	
80	28	200	160	8x⌀18
100	28	220	180	
125	28	250	210	
150	28	285	240	8x⌀23

Tab.3

* Innengeometrie und Treibnennweite werden betriebsintern, abhängig von der Leistung und dem Treibmittelzustand bestimmt. (KN 121021:...25)
Bitte geben Sie diese Daten im Bestellfall an.
Internal geometry and diameter of motive connection are determined by workshop, depending on the performance and on the motive fluid condition.
Please indicate these data in case of order.

Änderungen vorbehalten ! *Subject to change !*

Alle Rechte vorbehalten! Nicht genehmigte Weiterverwertung, insbesondere Nachahmung oder sonstiger Mißbrauch des geistigen Eigentums wird zivil– und strafrechtlich verfolgt!
All rights reserved. Unauthorised re–use, particularly imitation or other abuse of copyright, will be subject to legal proceedings.

1987 | Datum: Date | Name: Name
Bearbeitet: in charge | 06.08. | Hegricy
Genehmigt: Approved | 19.11.
Ausgabe: Issue | 19.11.

Revi./Dat. | 1 | 2 | 3 | 4 | 5 | 6 | 7 | 8

Figure 10 Specification for the ejector proposed by Körting

Funded by the European Union

2.4 CRMC design

The criterion proposed by Eames (2002) is based on the idea of suppressing the normal shock that is expected to take place in the cylindrical section typically located in the central part of the ejector. To achieve this, the author proposed to impose a constant rate of deceleration throughout the supersonic diffuser, which forms the main part of the ejector. The diffuser is hence designed as a duct with a continuously varying cross-section to accommodate the expanding flow. Since the inlet flow is supersonic, the resulting duct naturally will have a convergent-divergent shape, with the throat corresponding to a Mach number of unity. When operating precisely at the design reference point, the transition between supersonic and subsonic regimes should occur smoothly, without any shock.

Before discussing the equations of the CRMC design, it is necessary to address the mixing process, which precedes the deceleration stage. An ejector essentially acts as a "momentum exchanger", i.e., the mixed flow receives the sum of the motive and entrained flow momentum:

$$\dot{m}_{mix} c_{mix} = \dot{m}_m c_m + \dot{m}_s c_s$$

where the subscript *m* refers to the motive flow and the subscript *s* refers to the entrained flow. Since $\dot{m}_{mix} = \dot{m}_m + \dot{m}_s$, this can be expressed as:

$$(1 + \omega) c_{mix} = c_m + \omega c_s$$

Some authors (e.g. Huang et al. 1999) introduce a reduction factor on the left-hand side of this equation to account for energy losses during the mixing process.

The mixing process is rather complex and would require at least a two-dimensional model to capture the intricate flow structures at the interface between the motive and entrained flows (Figure 10). Our experience shows that an "under-expanded" nozzle, i.e., a nozzle with an exit pressure higher than that found in the receiver, performs better than an "over-expanded" one, where the exit pressure is below the receiver pressure. As illustrated in the upper part of Figure 11, the latter configuration generates two oblique shocks originating from the nozzle edge, which dissipate energy. On the other hand, the under-expanded nozzle shown in the lower part of Figure 11 produces Prandtl-Meyer expansion waves, which are far less dissipative. In other words, the expansion continues beyond the nozzle exit and assists in entraining the fluid within the receiver.

The nozzle mounted in our prototype, shown in Figure 6, is slightly under-expanded and has demonstrated significantly improved performance.

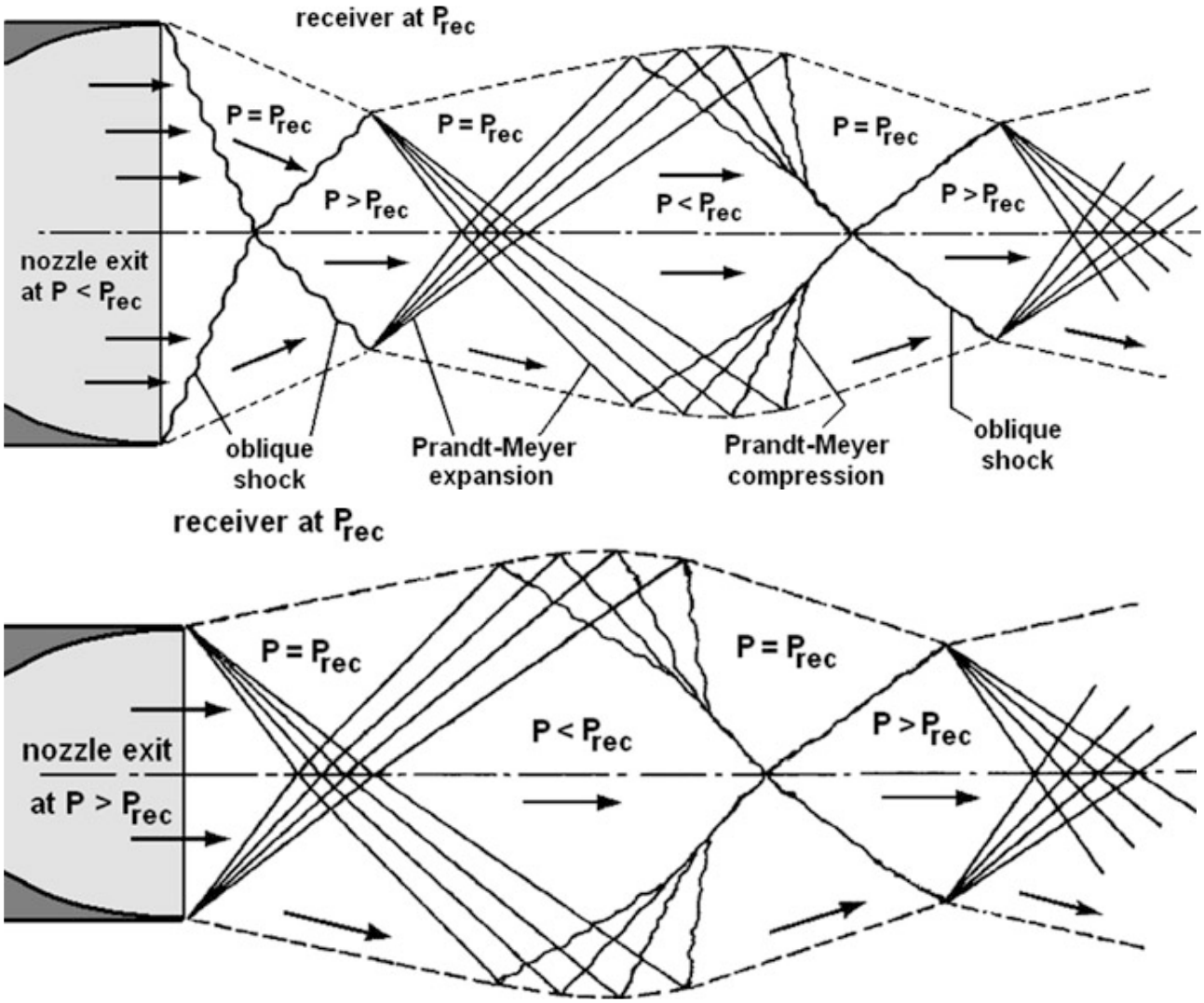

Figure 11 Expansion and compression waves at the motive nozzle exit: over-expanded (top) and under-expanded (bottom); from Zucker and Biblarz (2002)

In a previous publication (Grazzini, Milazzo and Mazzelli, 2018), our group presented a simplified approach in which the mixed flow is formed within a conical region downstream of the nozzle exit (Figure 12). The entrained flow, initially unaltered, gradually enters the cone, and the flow conditions evolve accordingly. The angle of the mixing cone is related, but not necessarily equal to, the nozzle angle. The choice of this angle determines the length of the mixing zone. Note also that the sharp distinction between the mixing zone and the diffuser is somewhat artificial, as the mixing in reality occurs throughout most of the ejector length.

The fundamental design specification for the system is a cooling capacity of 20 kW, which can be translated into a suction flow rate once the evaporator conditions are defined. The motive flow at start is unknown and depends on the actual entrainment ratio achieved by the ejector.

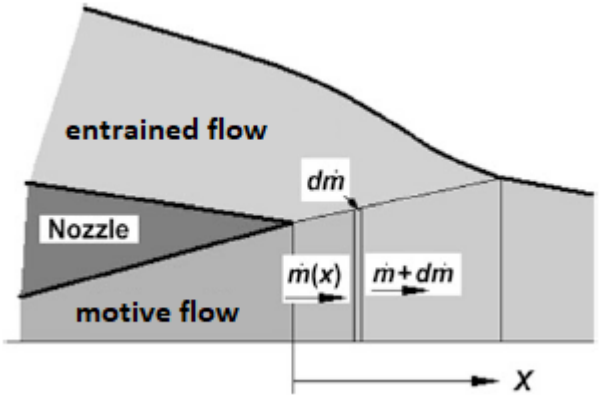

Figure 12 Simplified model of the mixing zone

Therefore, the CRMC procedure must be carried out prior to the design of the nozzle and mixing zone. Starting from the supersonic velocity c_{mix}, we assume a constant deceleration rate:

$$\frac{dc}{dz} = a$$

The length L of the diffuser is initially assigned a trial value, which will later be verified, as shown in the following sections. The initial velocity is c_{mix}, While the outlet velocity c_{out} is set to the minimum value that ensures adequate discharge through a reasonably sized ejector outlet. The velocity at any point along the diffuser can thus be expressed as:

$$c_z = c_{mix} - \frac{c_{mix} - c_{out}}{L} z$$

Assuming a horizontal diffuser, with negligible heat transfer and no external work, the energy balance gives:

$$cdc + dh = 0$$

Integrating this expression from the diffuser inlet gives a relation for enthalpy:

$$h_z = h_{mix} + \frac{c_{mix}^2}{2} - \frac{c_z^2}{2}$$

The initial enthalpy h_{mix} is obtained from an energy balance during the mixing process:

$$h_{mix} + \frac{c_{mix}^2}{2} = h_m + \frac{c_m^2}{2} + h_s + \frac{c_s^2}{2}$$

Conservation of mechanical energy further gives:

$$cdc + \frac{dP}{\rho} + Tds_{irr} = 0$$

where the last term accounts for the losses due to viscous friction within the fluid. A dimensionless friction factor f can be introduced in order to evaluate these losses:

$$Tds_{irr} = f \frac{dz}{D} \frac{c^2}{2}$$

Funded by the European Union

where D is the duct diameter. Substituting and solving yields the pressure gradient:

$$dP = -\rho\left(cdc + f\frac{dz}{D}\frac{c^2}{2}\right)$$

Evaluating the friction factor for two-phase flows is challenging, since the nozzle expansion produces some liquid, and the mixture may enter the two-phase region for water. However, given the high velocity of the flow in the nozzle, the condensed liquid fraction is usually small (though it strongly affects the steam temperature) and is further diluted as the motive and entrained flows mix. Furthermore, as the compression within the diffuser proceeds, the temperature rises and soon reaches the saturation limit, entering the superheated steam region. Therefore, the friction can be evaluated based on the prevailing vapor phase.

A well-known formula for the friction factor is that of Churchill (1977):

$$f = 8\left[\left(\frac{8}{Re}\right)^{12} + \frac{1}{(A+B)^{1.5}}\right]^{1/12}$$

where $A = \left\{2.457\ ln\left[\frac{1}{(7/Re)^{0.9}+0.27\varepsilon/D}\right]\right\}^{16}$ and $B = \left(\frac{37530}{Re}\right)^{16}$. The Reynolds number can be evaluated using the two-phase viscosity according to the McAdams formula:

$$\mu_{tp} = \frac{1}{\frac{x}{\mu_v} + \frac{1-x}{\mu_l}}$$

The relative roughness ε/D was evaluated assuming an average surface roughness Ra = 0.8 μm.

Once the enthalpy and pressure are determined, all other thermophysical properties can be calculated using, e.g., NIST REFPROP. The density $\rho(P,h)$ is then used to determine the local flow cross-sectional area:

$$A = \frac{\dot{m}_{mix}}{\rho c}$$

The use of real-fluid properties marks a departure from the original formulation by Eames (2002), which was based on the ideal gas law. As shown by Grazzini, Milazzo and Piazzini (2011), ideal-gas assumptions lead to unrealistic thermodynamic states, while classical nucleation theory predicts homogeneous condensation of droplets within the motive nozzle. Although the condensed mass fraction is small, the released latent heat significantly alters the state of the expanding steam and cannot be neglected.

REFPROP readily calculates the equilibrium state of the steam at any point. In practice, the condensation occurs with some delay relative to equilibrium predictions. However, this delay does not require specific design corrections, as the nozzle still exhibits high efficiency even in a simplified design. Beyond the nozzle, metastable effects are no longer significant.

For example, starting from the specifications in Table 1, assuming a nozzle efficiency of $\eta_{noz} = 0.95$, the resulting nozzle exit velocity is $c_m = 1137\frac{m}{s}$. The entrained flow enters the ejector at low velocity. However, its effect can be accounted for by slightly reducing the pressure in the mixing zone.

Funded by the European Union

By setting $\frac{dc}{dz} = 500\ s^{-1}$ and performing the calculations as described above, we obtain the results listed in Table 2.

Table 2 Results of the CRMC calculation

Entrainment ratio	0.637
Motive steam mass flow rate	0.0133 kg/s (47.9 kg/h)
Mixing pressure	985 Pa
Mixed flow rate	0.0217 kg/s (78.1 kg/s)
Length	1.41 m
Discharge temperature	75°C
Discharge velocity	15 m/s
Efficiency	0.9

Pressure and temperature profiles along the supersonic diffuser are shown in Figure 13. As can be clearly seen, the pressure (blue line) increases continuously until, at z = 1410 mm, it reaches the outlet pressure (red horizontal line), discharging the fluid toward the condenser with an exit velocity of 15 m/s.

The temperature rises to approximately 75 °C. A discontinuity in the slope of the temperature curve is evident in Figure 13b. This behavior is caused by the presence of liquid water droplets originating from the motive nozzle in the diffuser. Once the liquid has fully evaporated, the specific heat of the mixture changes markedly. This again demonstrates that the real thermophysical properties of steam must be taken into account.

The efficiency of the diffuser can be defined as:

$$\eta_{diff} = \frac{h_{id} - h_{mix}}{h_{out} - h_{mix}}$$

Substituting the values obtained from the CRMC diffuser calculation yields $\eta_{diff} = 0.9$. This result, being derived from purely thermodynamic reasoning, may be somewhat overestimated.

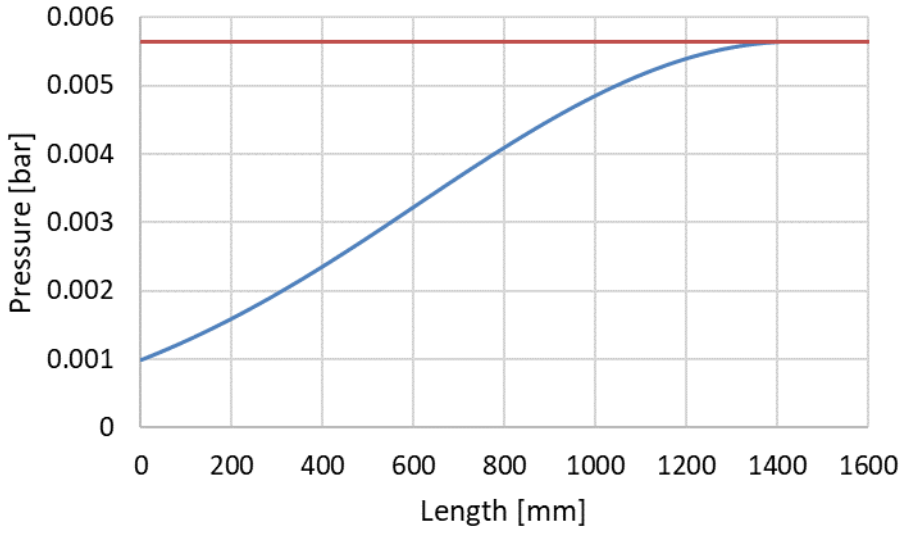

(a

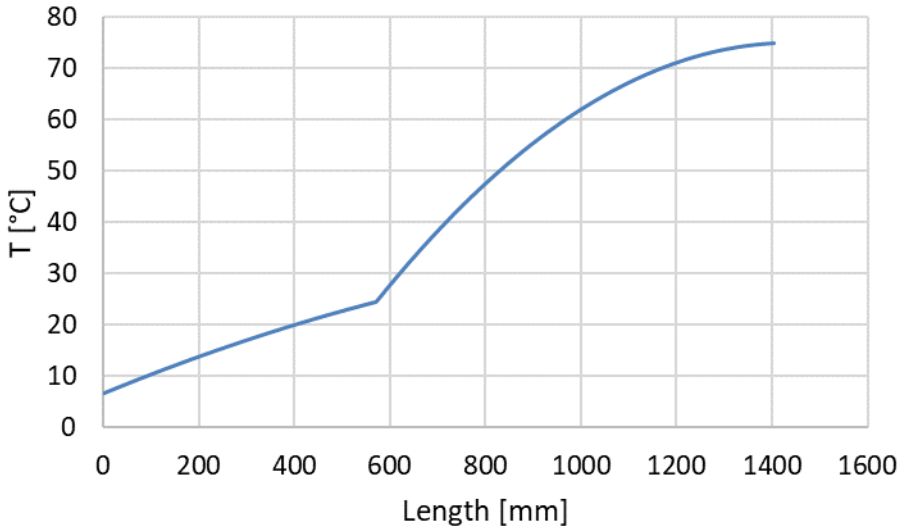

(b

Figure 13 *Pressure (a) and temperature (b) along the CRMC diffuser*

Plotting the radius of the section, we have the profile shown in Fig. 14.

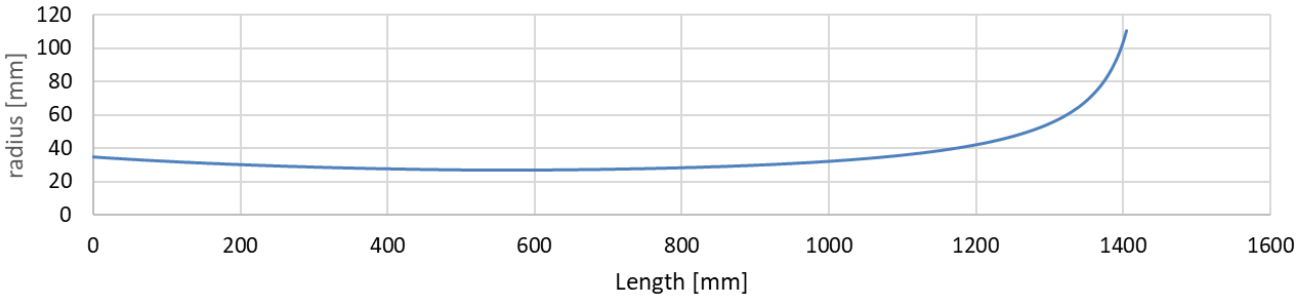

Figure 14 *Profile of the CRMC diffuser*

Note that the figure is not to scale, in order to enhance the visibility of the shape. The most striking feature is the strongly diverging outlet, which appears to contradict establihsed design practices. Based on our previous experience, this section of the profile should be corrected by adopting a smaller diverging angle. This and other adjustments will be detailed later, when all components of the ejector are presented together.

Additional relevant data are shown in Table 3.

Table 3 CRMC diffuser data

Section	Pressure [bar]	Density [kg/m^3]	Velocity [m/s]	Area [mm^2]	Diameter [mm]
Inlet	0.000985	0.00806	720	3740	69
Throat	0.003	0.0225	435	2207	53
Outlet	0.00563	0.0351	15	30700	197

In our previous experimental campaign, we measured the static pressure along the ejector using nine pressure transducers installed at 100 mm intervals, as shown in Figure 5.

As shown in Figure 15, the results differ significantly from those presented in Figure 13a. As an example, Figure 15 refers to a motive flow saturation temperature of 97 °C and an entrained flow saturation temperature of 2.5 °C. Since the working fluid is different, these results are only qualitative. Nevertheless, while awaiting the experimental results from the new ejector, they provide useful insight into the expected behavior.

The eight curves shown are grouped into a lower and upper bundle, each containing four curves. Each curve corresponds to a point in the small COP diagram in the lower right corner. The lower curves (points 1–4) represent the “on-design” operating condition. In these cases, the pressure shows a slight decrease from the value $P_{E\text{-}out}$ at the evaporator outlet (i.e., at the entrained flow inlet). The two leftmost transducers (X= 50 and 150 mm from the ejector inlet) record low pressures that are insensitive to the downstream conditions. A sharp increase appears at the third transducer (250 mm), where the pressure starts to rise and the constant-pressure mixing zone apparently ends. The pressure then rises steeply up to transducer no. 6 (X=550 mm). Beyond this point, it increases more moderately up to transducer no. 8, but decreases again at transducer no. 9, i.e., in the final conical section of the ejector. Instead of a further pressure recovery, this last portion produces a slight pressure loss.

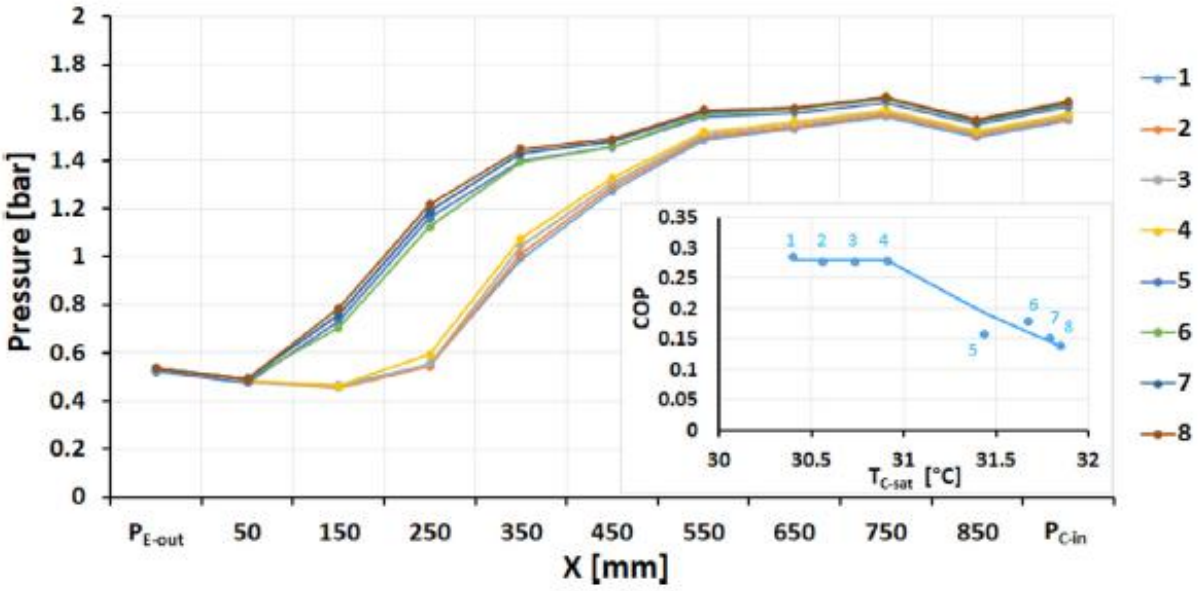

Figure 15 Measured pressure along the ejector shown in Figure 5 – Working fluid R1233zd (Mahmoudian et al., 2021)

The upper four curves show a completely different behaviour. They correspoind to "off-design" conditions in which all transducers are affected by the downstream pressure. In these cases (points 5–8 in the graph), the critical saturation temperature at the condenser has clearly been exceeded.

Although the CRMC model shows some discrepancies compared with the measured ejector behavior, our ejector chiller has demonstrated high efficiency. Unfortunately, an equivalent ejector based on a traditional design was never built for comparison. Therefore, we rely on the results published by Kitrattana, Aphornratana and Thongtip (2023), which demonstrate that the CRMC design procedure, although not perfectly reproducing reality, can nevertheless yield an efficient ejector.

2.5 Design of the motive nozzle

Once the motive flow rate has been determined, the design of the motive nozzle can be carried out. This task is performed in an innovative manner compared to the conventional gas-dynamic approach based on the Mach number. Again, given the presence of condensation, the steam cannot be treated as an ideal gas.

The nozzle throat is determined directly from its definition: for a constant mass flow rate, the minimum cross-sectional area corresponds to the maximum value of the product of density and velocity:

$$A_{min} = \frac{\dot{m}}{(\rho c)_{max}}$$

Funded by the European Union

Starting from the inlet velocity, which may be assumed as $c_0 = 10\ m/s$, and the inlet enthalpy h_0 corresponding to the saturation condition at 130 °C, the value of $(\rho c)_{max}$ is searched over the pressure range between the inlet and outlet of the nozzle.

For the motive nozzle, estimating the friction factor as done for the diffuser would be inappropriate, as the duct is very short and its flow area varies considerably. Instead, a nozzle efficiency η_{noz} is introduced by calculating an ideal enthalpy h_{id} for isentropic expansion and the corresponding real enthalpy:

$$h = h_0 - \eta_{noz}(h_0 - h_{id})$$

The fluid density is again calculated using REFPROP as a function of pressure and enthalpy, while the velocity is obtained from the energy balance:

$$c = \sqrt{c_0^2 + 2(h_0 - h)}$$

The pressure value corresponding to $(\rho c)_{max}$ defines the critical pressure. Applying the Fibonacci search method for the maximum, we have $P_{crit} = 1.56$ bar.

At this point, the three characteristic sections of the nozzle can be determined. The results are shown in Table 4.

Table 4 Motive nozzle data

Section	Pressure [bar]	Density [kg/m^3]	Velocity [m/s]	Area [mm^2]	Diameter [mm]
Inlet	2.7	1.497	10	953.4	34.84
Throat	1.56	0.924	426	35.2	6.79
Outlet	0.001	0.00975	1136	1289	38

These three sections can be connected using any profile that ensures a short converging part, a rounded throat, and a diverging part with a small angle, in order to avoid flow separation along the nozzle wall. The inlet section diameter may be rounded up to 35 mm, as the inlet velocity (10 m/s) is purely conventional and has a limited effect on the nozzle performance.

Based on our previous experience, two Bézier functions connected at the throat are well suited for defining the nozzle profile. This approach allows precise close control of both the slope and curvature in the critical sections of the nozzle. On the inlet side, the profile should align smoothly with the straight tube carrying the motive steam. At the throat, the convergent and divergent sections should have matching first derivatives to prevent any flow detachment. A further refinement is to ensure continuity of the second derivative, thereby achieving a smooth transition not only in direction but also in curvature.

The Bézier curve is defined as:

$$B(t) = (1-t)^3 P_0 + 3(1-t)^2 t P_1 + 3(1-t) t^2 P_2 + t^3 P_3$$

where t is a parameter ranging from 0 to 1, and $P_0, P_1, \ldots$ are four control points that determine the position and slope at the endpoints of the curve. By coupling two Bézier curves that share a terminal point and have their control points aligned and symmetric with respect to that point, the desired nozzle profile can be obtained (Figure 16). The control points are shown in purple.

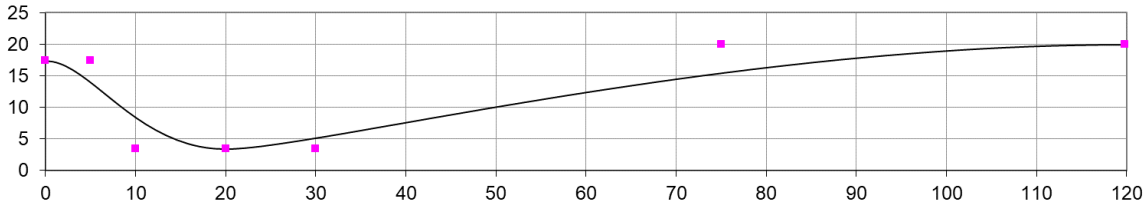

Figure 16 Profile of the motive nozzle (not to scale).

This design was used in our ejector chiller prototype (as shown in Figure 6) and produced very good results. A 0.2 mm-radius fillet terminates the profile to prevent a sharp and fragile edge. The outer contour is cylindrical, ending in a short conical section.

The final configuration is shown in Figure 17. The details of the connection between the nozzle and the pipe carrying the motive steam will be defined later.

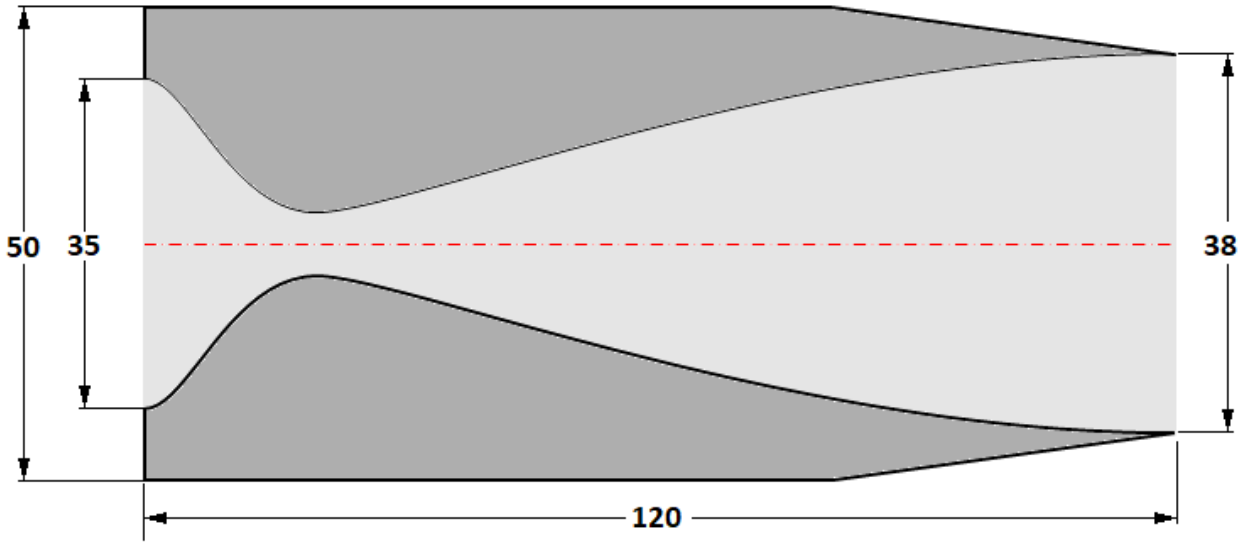

Figure 17 Section of the motive nozzle

2.6 Design of mixing chamber

The mixing process has already been modelled to determine the fluid state at the inlet of the diffuser. Here, we describe the design of the profile of this chamber, which constitutes the first part of the ejector.

The inlet section must be large enough to accommodate the motive nozzle, which, as shown in Figure 17, has an outer diameter of 50 mm. In close cooperation with RIVACOLD, it was found that

a diameter of 150 mm allows the use commercially available components (connections, fittings, etc.), while larger dimensions would introduce significant practical difficulties. Therefore, this diameter was adopted.

The flow area for the entrained flow at the nozzle exit plane is hence

$A_s = \frac{\pi}{4}(150^2 - 40^2) = 16414\, mm^2$.

As noted earlier, the entrained mass flow rate is $\dot{m}_s = 0.008449 \frac{kg}{s}$, and the density of saturated steam at 7 °C is $\rho_s = 0.00776 \frac{kg}{m^3}$. Hence, the corresponding velocity is $c_s = 66.4 \frac{m}{s}$.

The criterion described in Figure 11 provides a profile that can accommodate the entrained flow as it decreases from its full flow rate to zero. The flow area for the entrained stream is constructed around the cone that contains the mixed flow. However, this configuration produces a sharp corner in the profile at the junction with the upstream cylindrical section and with the CRMC profile described earlier.

Therefore, to prevent flow recirculation, the mixing section was instead designed to ensure a smooth and continuous profile throughout, achieved by applying an additional Bézier curve. The length of this section was set to 200 mm. The first two control points are aligned horizontally, while the last two are aligned with the derivative of the CRMC profile at the inlet.

As shown in Figure 18, the junction between the two sections, located at x=0, is perfectly smooth.

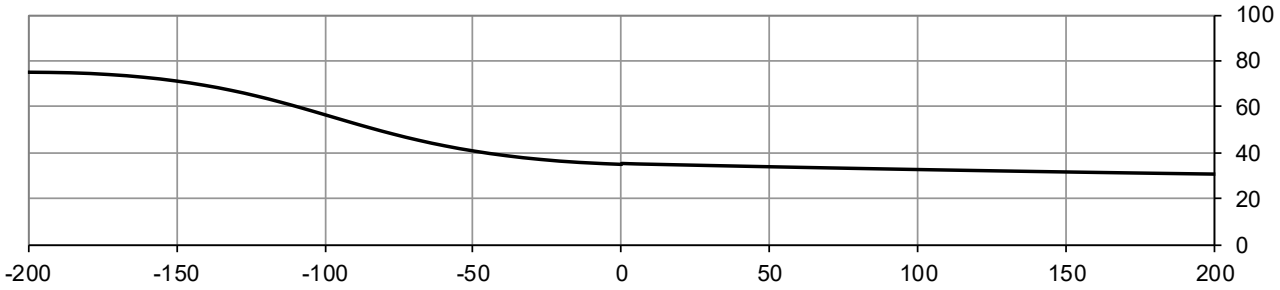

Figure 18 Profile of the inlet part of the ejector.

As stated earlier, the distinction between the mixing section and the CRMC diffuser is purely conventional, since the mixing in fact continues well beyond the junction at x=0. This will be illustrated later through CFD simulations.

2.7 Design of the end section

As stated earlier, the final part of the ejector shown in Figure 14 is clearly questionable from a design perspective. The flow will inevitably separate somewhere along the diffuser, dissipating energy through recirculation. Figure 19, adapted from Kitrattana, Aphornratana and Thongtip (2023), presents a CFD simulation of their ejector that illustrates this phenomenon.

The figure is vertically divided into two parts: the lower part shows the CRMC profile, while the upper part corresponds to the traditional design. Both configurations exhibit a separation zone. The traditional profile displays a longer separation region, while the CRMC profile has a shorter one. However, the volume occupied by the recirculating flow may be comparable in both cases.

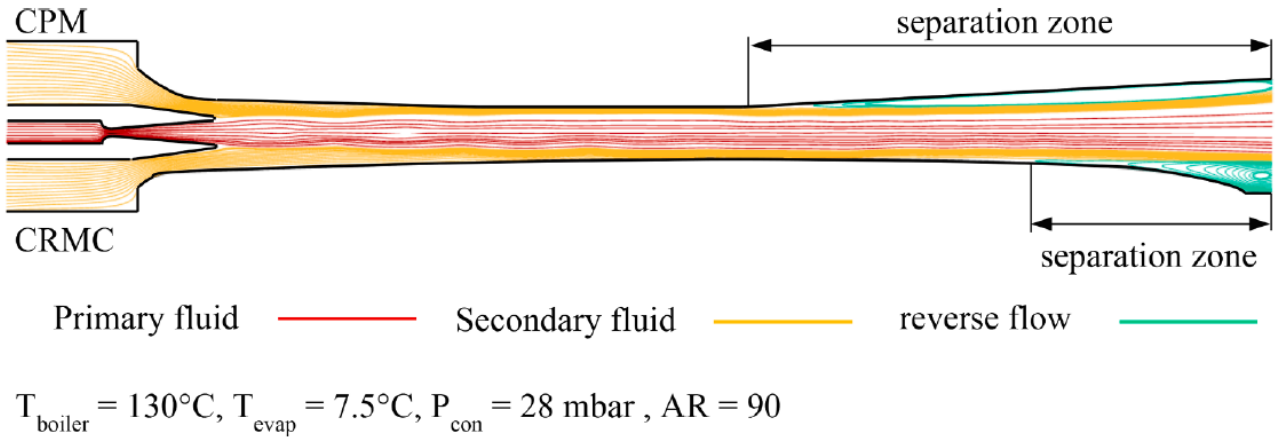

Figure 19 Flow separation at ejector end (from Kitrattana et al. 2023)

To mitigate this issue, the CRMC profile was modified in the end section. The curve was cut at 1200 mm from the inlet and replace by another Bézier curve, tangent to the original profile at the junction and horizontal at the outlet. The resulting profile is shown in Figure 20.

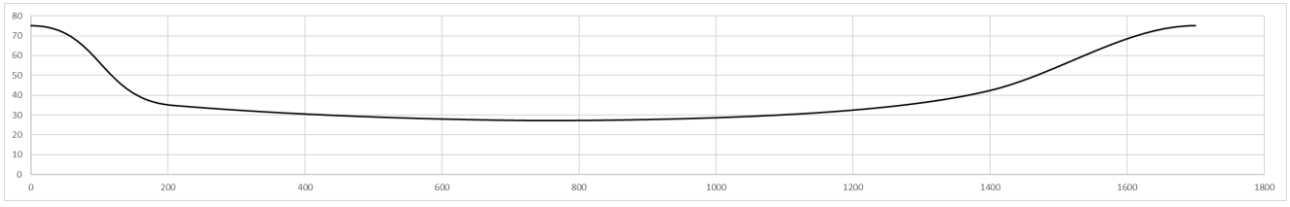

Figure 20 Complete profile of the ejector

Note that this design is not to scale. Both ends of the ejector have a radius of 75 mm, corresponding to a diameter of 150 mm, which allows easy connection with the other components of the circuit.

2.8 Assembly of the complete ejector

The motive nozzle and the ejector body are combined in a final assembly schematically shown in Figure 21. Again, the figure is not to scale. The outer contour of the ejector is only indicative, assuming a constant wall thickness of 10 mm. The exact shape will be defined later, taken into account requirements for holding the component during internal machining, positioning the pressure transducers, fitting other sensors, and so on.

It is likely that achieving the required high-quality internal surface finish will necessitate subdividing the ejector body into two or more parts, as was done in our previous ejector prototype (Figures 5 and 6). In this case, however, the connection between the parts must be designed to ensure perfect alignment.

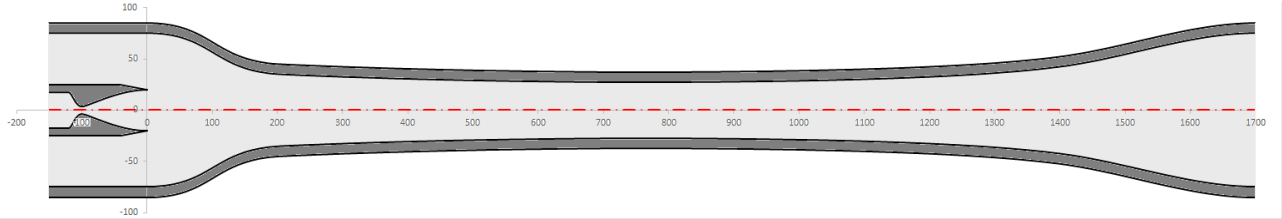

Figure 21 Assembly of the complete ejector (coordinate system centered at the nozzle exit)

2.9 Expected performance of the cooling cycle

Based on the calculations performed, the expected performance of the ejector chiller is:

$$COP = \omega \frac{h_E - h_A}{h_G - h_A} = 0.637 \frac{2514 - 146.6}{2720 - 146.6} = 0.586$$

Another key performance parameter is the motive steam consumption:

$\dot{m}_m = 0.0133 \frac{kg}{s} = 47.8 \frac{kg}{h}$.

This steam consumption is clearly much lower than that estimated by Körting in their offer.

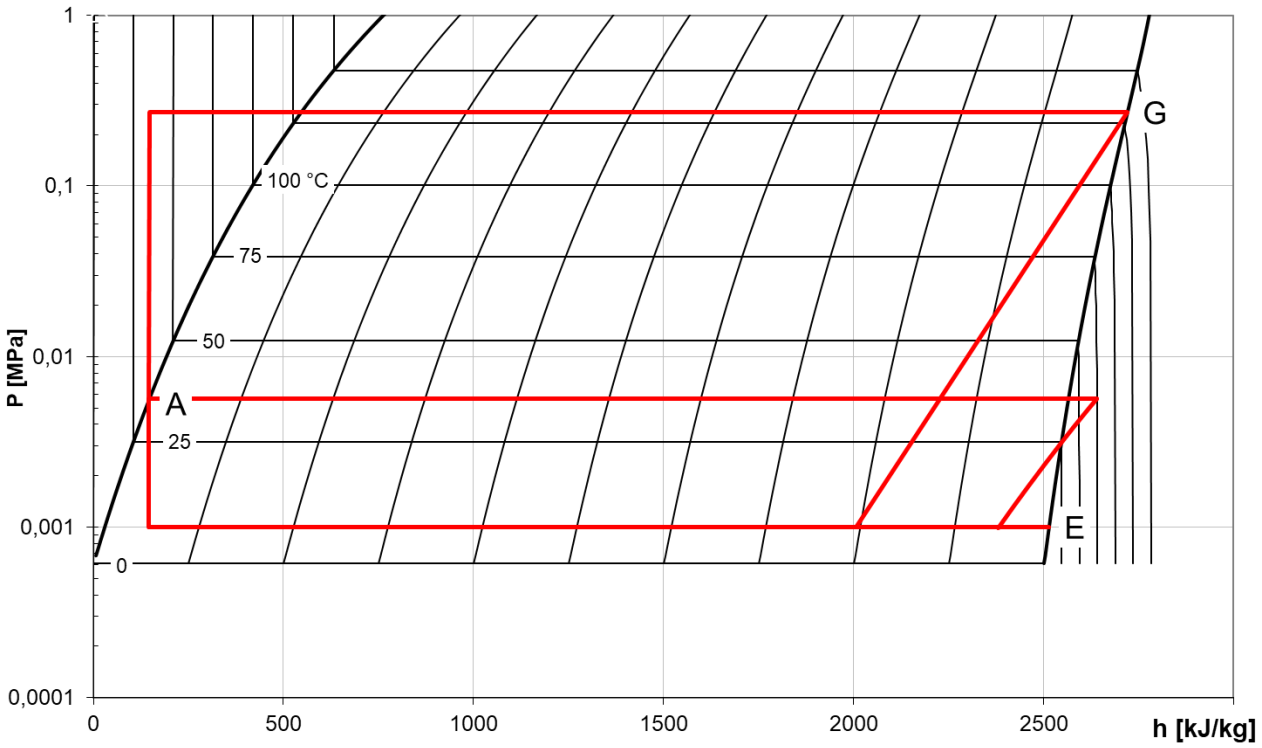

Figure 22 *P–h diagram of the calculated cycle*

Figure 23 *T–s diagram of the calculated cycle*

Funded by the European Union

Note that in the P–h diagram shown in Figure 22, the slight pressure difference due to the acceleration between the evaporator (point E) and the nozzle exit plane is not visible.

The cycle is also shown in the T–s diagram of Figure 23. Point m and s correspond to the motive and entrained flow conditions at the nozzle exit. Again, point E (evaporator outlet) and point s, representing the fluid condition after accelerating to 66 m/s, are indistinguishable, as the temperature difference is only 0.01 °C.

The line connecting point “mix” and point C (condenser inlet) consists of 280 points obtained from the CRMC ejector calculation. A distinct change in slope can be observed where the line crosses the boundary between saturated and superheated steam.

The line from G to m, on the other hand, is a straight line representing the entropy increase associated with the non-unit efficiency of the motive nozzle ($\eta_{noz} = 0.95$).

2.10 Response to variation in the operating conditions

Ejectors are generally considered to be quite rigid with respect to changes in the operating conditions. The key parameter that can be adjusted to accommodate varying boundary conditions is the ratio between the ejector throat and nozzle throat diameter. In the present design, this ratio is:

$$\Psi = \frac{D_{ejector}}{D_{nozzle}} = \frac{53}{6.79} = 7.8$$

As a rule, a higher Ψ ratio increases the entrainment ratio but decreases the critical condensation temperature. Therefore, during colder seasons, it may be advantageous to use a nozzle with a smaller throat diameter. However, replacing the nozzle requires opening the circuit and subsequently restoring the vacuum.

An alternative approach is to reduce the nozzle throat area using a spindle that can move longitudinally, as originally implemented in Giffard’s injector in 1850 (see Figure 3). An electric or hydraulic actuator could be installed inside the sealed circuit and operated without opening it. Although this introduces additional complexity into the cooling system, it could significantly improve its seasonal efficiency.

2.11 Role of wall roughness and heat exchange

In Mazzelli & Milazzo (2015), we demonstrated that the wall roughness has a significant effect on the ejector performance. While the entrainment ratio under on-design conditions is not strongly affected by wall friction, friction losses have a major impact on the onset of off-design operation, thereby reducing the critical pressure.

In the present project, the ejector will be manufactured in aluminum using high precision CNC machine tools. The surface roughness assumed forthis design (Ra = 0.8 μm) is undoubtely a good quality, although even smoother surfaces can now be achieved with modern machining.

Given the relatively low mechanical and thermal stresses acting on the ejector body, the use of plastic materials could also be considered. The first ejector mounted on our chiller prototype was manufactured from carbon-fiber composite. The composite was formed around a male steel mold that could easily be superfinished, resulting in a very smooth internal surface. Much less expensive composite materials could also be employed.

Another aspect that is often overlooked in ejector research is heat transfer. The aforementioned carbon-fiber ejector was imaged using an infrared camera (Figure 24), revealing a sharp thermal gradient between the inlet section (left), where the wall is in contact with the cold fluid from the evaporator, and the outlet section (right), where it is exposed to the compressed fluid flowing toward the condenser. In this case, the material's moderate thermal conductivity and good emissivity made it particularly suitable for thermal imaging.

This image clearly shows that the assumption of adiabaticity is far from realistic. Neverthelessd, the present project does not, for the moment, deviate from the commonly accepted adiabatic approach. It should also be noted that the expected discharge temperature will be higher when operating with steam compared to R245fa, which was the working fluid used when this image was recorded.

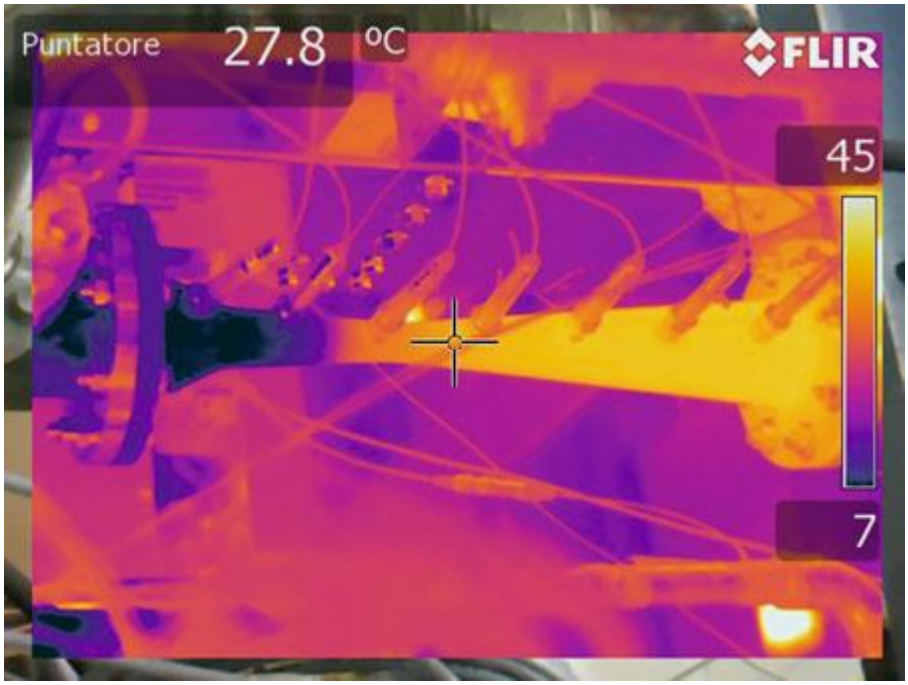

Figure 24 Infrared picture of the carbon fiber ejector on our prototype

In the case of an aluminum ejector, the longitudinal thermal conductivity is expected to be significantly higher. This could lead to a more uniform wall temperature, transferring heat from the hot to the cold region, which is likely to deteriorate the ejector's performance.

Unfortunately, incorporating heat transfer into the model is challenging, as it requires a coupled fluid-solid simulation. If feasible, this aspect will be investigated in future work. In addition, wall

temperature measurements will be carried out to provide sufficient data for validating the computational analysis.

3 Design of the flash evaporator

3.1 Motivations for a flash evaporator

In our previous prototype, the evaporator consisted of a plate heat exchanger. This configuration introduced a temperature difference between the evaporating fluid and the cooling medium ultimately serving the cooling load.

In larger ejector chillers, flash evaporators are commonly used, offering improved efficiency. The cooling system illustrated in Figure 25 also includes a double-stage ejector and a barometric condenser. This latter eliminates the need for the pump that would normally be required to return the condensate to the steam boiler. It should be noted that this configuration is only feasible when the working fluid is water, owing to the relatively low pressure at the steam boiler and the high density of the liquid phase.

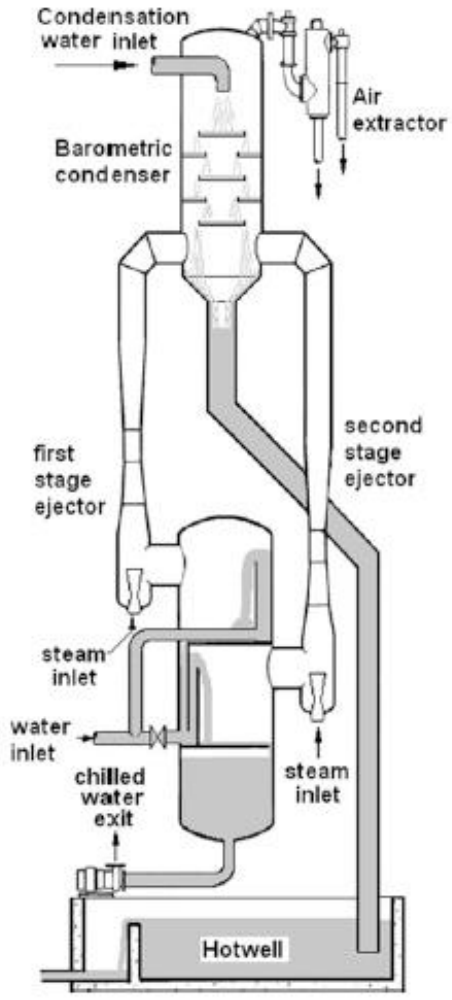

Figure 25 Steam jet industrial cooling plant

This configuration is undoubtedly the least expensive option for a heat-powered cooling cycle. However, the direct contact between water and air introduces non-condensable gases, which dissolve in the water and must be removed from the condenser. In the system shown in Figure 25, this task is carried out by an additional ejector acting as an air extractor.

In our design, the water circuit serving the cooling load will be completely closed. A pump located below the flash evaporator (Figure 2) will raise the water to atmospheric pressure to minimise air infiltration along the line. The pressure difference created by this pump is then used to atomize the spray as the water returns to the evaporator. Additional spray nozzles are employed to atomize the water returning from the condenser.

The water collected at the bottom of the flash evaporator functions as a fluid reservoir, helping to buffer small load fluctuations.

3.2 Design constraints

A first obvious constraint concerns the mechanical strength of the evaporator envelope with respect to the pressure difference between the inside and the outside. For simplicity and safety, this pressure difference can be assumed to be equal to 1 atm.

Another important consideration is the risk of liquid water entrainment by the raising steam flowing toward the ejector. To avoid this, a suitable height difference must be maintained between the spray nozzles and the ejector inlet and the upward velocity of the vapor must be limited.

3.3 Design results

The design was carried out by RIVACOLD, based on their experience with liquid receivers in vapor-compression refrigeration systems. The results are shown in Table 5.

Table 5 Main features of the flash evaporator

Height L	1500 mm
Internal diameter IDS	400 mm
Height H2	480 mm
Height H1	760 mm
Max level	470 mm
Min level	370 mm
Liquid volume	100 l

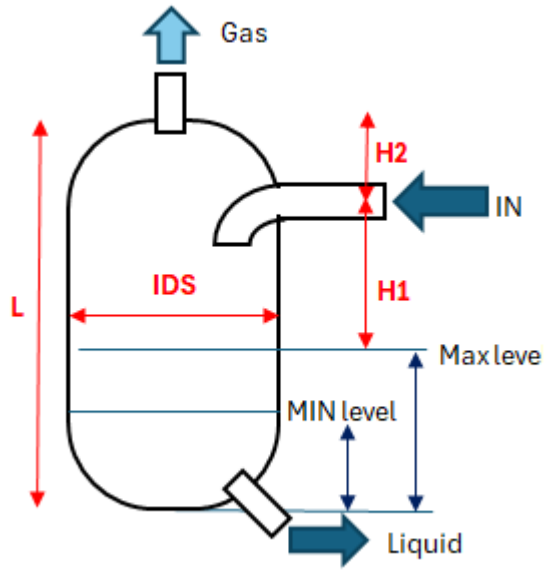

Figure 26 Scheme of the flash evaporator as a liquid separator

4 Design of the condenser

4.1 Design constraints

The condenser must operate at sufficiently low pressure to allow the discharge of steam from the ejector. The heat power that the condenser must discharge to the environment is:

$$\dot{Q}_{out} = \dot{m}_{mix}(h_C - h_A) = 54.1\ kW$$

Which, as expected, is the sum of the cooling power $\dot{Q}_{cool} = 20\ kW$ and the motive steam power $\dot{Q}_m = 34.1\ kW$.

The condensing pressure is governed by the ambient temperature and by the thermal resistance between the condensing fluid and the surroundings. Increasing the heat-exchange surface reduces the thermal resistance but also increases the overall cost of the system.

The condensing temperature assumed in the previous calculations (35 °C) is sufficiently high to accommodate typical environmental conditions in Italy. Under very high ambient temperatures, the condenser performance can be improved by spraying water onto the heat-exchanger surface or onto a porous layer that pre-cools the air before it enters the heat exchanger. In this way, the inlet air temperature can approach the wet-bulb temperature, which in Italy is normally below 25°C. Additional performance enhancement can also be obtained by using a cooling tower.

5 Design of the system layout

A schematic layout of the system is shown in Figure 25. This configuration has been designed for the first experimental phase, which will take place in the RIVACOLD laboratory. The condensation occurs in a plate heat exchanger cooled by the centralized cooling system serving the labs.

The pumps, which will be selected by RIVACOLD, should be installed as far as possible below the evaporator and the condenser to prevent cavitation. If necessary, side-channel pumps or other types not prone to cavitation will be employed.

The entire circuit must be airtight to prevent air infiltration, as any trapped air would accumulate in the condenser and raise its pressure, reducing the ejector's performance. On the other hand, this system will not be affected by the presence of humidity in the working fluid, unlike conventional refrigeration systems.

The layout will be modified when the system is transferred to S.M.F. for field testing.

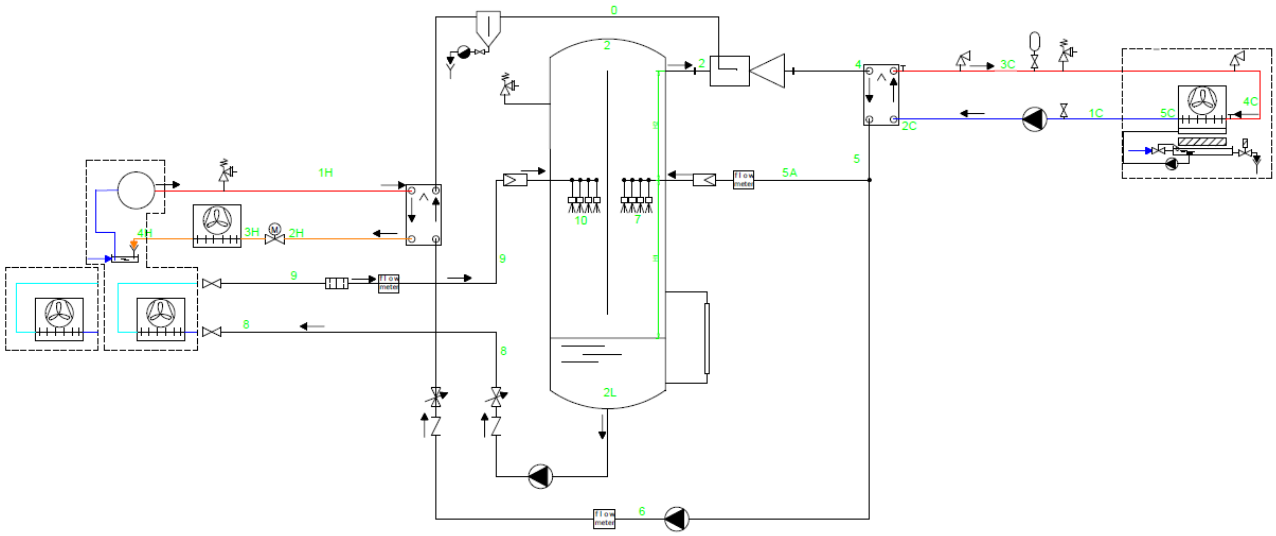

Figure 27 System layout

Funded by the European Union

6 Conclusions

The system outlined in this study exhibits good performance (COP = 0.586) despite the demanding environmental specifications. In locations with lower ambient temperatures, the system performance would be even higher. To fully exploit this potential, a control system capable of adjusting the ejector diameter ratio Ψ should be employed.

Naturally, the results obtained from the thermodynamic simulations must be verified experimentally and may prove slightly optimistic. A realistic performance target would be COP = 0.5.

The system features a simple construction, with no moving parts other than the pumps. As such, it could compete effectively with other heat-powered refrigeration systems, such as lithium bromide absorption chillers. The initial investment cost is expected to be lower, being mainly associated with the heat exchangers (i.e. the condenser and the heat exchangers in the cooled space).

The working fluid is pure water, with a Global Warming Potential (GWP) of 0 and safety class A1 (non-toxic, non-flammable). Compared with water/LiBr solutions, issues related to corrosion and gas release from chemical reactions are eliminated.

However, the full potential of the GEOSYN concept will only be fully exploited once the integration with the high-temperature heat pump is successfully demonstrated.

7 References

Besagni, G., Mereu, R., Inzoli, F., (2016). Ejector refrigeration: A comprehensive review. Renew. Sustain. Energy Rev. 53, 373–407.

Eames, I, (2002). A new prescription for the design of supersonic jet-pumps: The constant rate of momentum change method. Applied Thermal Engineering, 22, 121-131

Grazzini, G., Milazzo, A., Mazzelli, F., (2018). Ejectors for Efficient Refrigeration. Springer.

Grazzini, G., Milazzo, A., Piazzini S., (2011) Prediction of condensation in steam ejector for a refrigeration system, International Journal of Refrigeration, 34, 1641-1648

Grazzini, G., Rocchetti, A., (2002), Numerical optimisation of a two-stage ejector refrigeration plant, International Journal of Refrigeration 25 (2002) 621–633

Huang, B., Chang, J., Wang, C., & Petrenko, V. (1999). A 1-D analysis of ejector performance. International Journal of Refrigeration, 22, 354–364

Kitrattana B., Aphornratana S., Thongtip T., (2023) Investigation on improvement potential of steam ejector performance in refrigeration cycle via constant rate of momentum change design method, Applied Thermal Engineering 231 (2023) 120953

Mahmoudian J., Rocchetti A., Mazzelli F., Milazzo A. (2021) A heat-powered ejector chiller working with low-GWP fluid R1233zd(E) (Part 1: Experimental results), International Journal of Refrigeration, 121 1–9

Mazzelli, F., Milazzo, A., (2015). Performance analysis of a supersonic ejector cycle working with R245fa. Int. J. Refrig. 49, 79–92 .

Routledge R., (1876). Discoveries and inventions of the nineteenth century. George Routledge & Sons, London

“Geothermal Heating & Cooling for Industry

APRE

UNIVERSITÀ DEGLI STUDI FIRENZE | DIEF DIPARTIMENTO DI INGEGNERIA INDUSTRIALE

COSVIG

SDU

Geothermal UKRAINE

SINTEF

RIVACOLD MASTERING COLD

neo-eco

FORMAGGERIA TOSCANA

www.geosynproject.eu

info@geosynproject.eu

#GEOSYNPROJECT

Funded by the European Union